CLINT

CLIMATE INTELLIGENCE

EXTREME EVENTS DETECTION

December 2022

This project is part of the H2020 Programme supported by the European Union, having received funding from it under Grant Agreement No 101003876

Programme Call:	Building a low-carbon, climate resilient future: climate action in support of the Paris Agreement (H2020-LC-CLA-2018-2019-2020)
Grant agreement ID:	101003876
Project Title:	CLINT
Partners:	POLIMI (Project Coordinator), CMCC, HZG, CSIC, SMHI, HKV, E3M, TCDF, DKRZ, IHE, ECMWF, UAH, JLU, OGC, UCM
Work-Package:	WP3
Deliverable #:	D3.1
Deliverable Type:	Document
Contractual Date of Delivery:	30 December 2022
Actual Date of Delivery:	28 December 2022
Title of Document:	Extreme Events Detection
Responsible partner:	ECMWF
Author(s):	Linus Magnusson, Michael Maier-Gerber, Enrico Scoccimarro, Veronica Torralba, Carmen Alvarez-Castro, Leone Cavicchia, Paolo Lanteri, Elena Xoplaki, Eduardo Zorita, David Barriopedro, Odysseas Vlachopoulos, Niklas Luther, Andrej Ceglar, Andrea Toreti, Matteo Giuliani, Ricardo Francisco Garcia Herrera, Claudia Bertini, Schalk Jan van Andel, Celia Ramos Sanchez, Lucia De Stefano, Yiheng Du, Wei Yang, Ilias Pechlivanidis, Dorien Lugt, Michiel Pezij, Martina Merlo, Andrea Castelletti.
Content of this report:	Description of the benchmark for Extreme Events detection: Indices and data to be used to detect the different kinds of Extreme Events considered in WP3 are described in the present document.
Availability:	This report is public.

Document revisions		
Author	*Revision content*	*Date*
Enrico Scoccimarro	D3.1_v01 – First draft of deliverable	25/10/2022
Linus Magnusson	D3.1_v02 – First revision	28/10/2022
Elena Xoplaki and JLU team	D3.1_v02_EX – Second revision	15/11/2022
Linus Magnusson	D3.1_v03 Added Introduction and Executive Summary	16/11/2022
Veronica Torralba	D3.1_v04 D3.2 revision	16/11/2022
Matteo Giuliani, Claudia Bertini, Schalk Jan van Andel, Celia Ramos Sanchez, Lucia De Stefano, Dorien Lugt, Michiel Pezij, Martina Merlo, Yiheng Du, Ilias Pechlivanidis	D3.1_v05 – analysis of historical droughts	18/11/2022
Enrico Scoccimarro	D3.1_v06 final internal revision	21/11/2022
Veronica Torralba	D3.1_v07 final formatting	25/11/2022
Nils Hempelmann	D3.1_v08 internal revision	02/12/2022
Wei Yang	D3.1_v09 internal revision	09/12/2022
Leone Cavicchia	D3.1_v10 internal revision integration	15/12/2022
Enrico Scoccimarro	D3.1_v11 internal revision integration	16/12/2022
Elena Xoplaki, Niklas Luther	D3.1_v12 internal revision integration	18/12/2022
Andrea Castelletti, Elena Matta	Final check and submission	28/12/2022

Table of Content

LIST OF FIGURES

LIST OF TABLES

LIST OF ACRONYMS

Abbreviations

WP: Work Package
ACRE: Atmospheric Circulation Reconstructions over the Earth
AI: Artificial Intelligence
AMO: Atlantic Multidecadal Oscillation
CAP: Common Agricultural Policy
C3S-CDS: Copernicus Climate Change Service – Climate Data Store
CIRES: Cooperative Institute for Research in Environmental Science
CMCC: Centro Euro-Mediterraneo sui Cambiamenti Climatici
CMIP6: Coupled Model Intercomparison Project Phase 6
ECMWF: European Centre for Medium-Range Weather Forecasts
EDA: Ensemble of Data Assimilations
EE: Extreme Events
EEA: European Environment Agency
EEcA: European Economic Area
EFTA: European Free Trade Association
ENSO: El Nino Southern Oscillation
EOF: Empirical Orthogonal Function
ERA5: ECMWF Reanalysis v5
ET: Extratropical transition
HYPE: HYdrological Predictions for the Environment
HydroGFD: Hydrological Global Forcing Data
FAO: Food and Agriculture Organization of the United Nations
GA: Grant Agreement
GAINS: Greenhouse Gas – Air Pollution Interaction and Synergies
GHG: Greenhouse Gas
GLOBIOM: Global Biosphere Management Model
GMES: Global Monitoring for Environment and Security
GPI: Genesis Potential Index
HMD: Heat Wave Magnitude
HW: Heat Waves
HWS: Heat Wave Severity
hPa: Hectopascal
IFS: Integrated Forecasting System
IOD: Indian Ocean Dipole
MJO: Madden-Julian Oscillation
ML: Machine Learning
MPI: Maximum Potential Intensity
NAO: North Atlantic Oscillation
NOAA: National Oceanic and Atmospheric Administration

NTUA: National Technical University of Athens
NWP: Numerical Weather Prediction
OLR: Outgoing Longwave Radiation
PDO: Pacific Decadal Oscillation
PMIP4: Paleoclimate Modelling Intercomparison Project phase 4
RES: Renewable Energy Sources
SMHI: Swedish Meteorological and Hydrological Institute
SPEI: Standardised Precipitation and Evapotranspiration Index
SPI: Standardised Precipitation Index
SRI: Standardised Runoff Index.
SSI: Standardised Soil Moisture Index
SST: Sea Surface Temperature
TC: Tropical Cyclone
TN: Tropical Nights

EXECUTIVE SUMMARY

In Machine Learning (ML), an essential part of the work is to define the training data set, both in terms of the target variable and the predictors. Once an ML model is constructed, one should benchmark it against an existing prediction model to validate its benefit. Therefore, one must consider the selection of datasets before developing the ML method.

This deliverable aims to describe indices and data to be used to detect the different types of Extreme Events (EE) considered in CLINT. The extreme events are:

- Tropical cyclones, in terms of genesis and activity on different timescales and extratropical transitions.
- Heatwaves and tropical nights
- Extreme droughts
- Compound events and concurrent extremes

For each type of EE, the report gives an overview of the problem, lists relevant indices and datasets, and discusses candidate drivers. The selection is based on a comprehensive review of current literature on each topic.

For tropical cyclones, local drivers for predictability, such as sea surface temperature (SST), moisture and vertical wind shear, will be combined with teleconnections of the Madden-Julian Oscillation (MJO) and the El Nino- Southern Oscillation (ENSO) to predict tropical cyclone activity at the sub-seasonal scale. On the climate scale, the genesis potential index (GPI) will be improved to detect cyclone activity.

For heatwaves and tropical nights over Europe atmospheric conditions such as flow regimes (NAO and blocking) together with remote oceanic, land and sea ice will be explored to predict the extreme events.

For extreme droughts, a combination of precipitation indices and hydrological models will be used to detect the event. To predict the extreme drought, similar drivers as for the heatwaves will be explored.

For compound events and concurrent extremes, ML will be utilised to detect events based on their impact on the water, food and energy sectors, derived from observations and impact models and appropriate combinations of precipitation and temperature indices.

The insights from this report will be used as input for the ML models that will be developed in the next stage of the CLINT project.

1 INTRODUCTION

In Machine Learning (ML) an essential part of the work is to define the training data set, both in terms of the target variable and the predictors. After constructing an ML model, one should benchmark it against an existing prediction model to validate the benefit. Therefore, one must consider the choices of datasets before building the ML method.

To obtain a good ML model, a sufficiently long training period with consistent data is needed. For this purpose, re-analyses (e.g., ERA5) are often used as they are produced with the same method for a long period. For observational time series, such consistency is harder to obtain as observation practices might have changed over time and space. However, the drawback with reanalysis products is that they partly build upon model approximations and may also suffer from non-stationarity issues in input observations.

Different types of problems require different solutions in terms of the type of predictors to use to train the model. The first distinction is whether an event is to be detected when it happens (e.g., whether there is a drought), or an event is to be predicted ahead of time (e.g., the genesis of a tropical cyclone). While local predictors are crucial for detection, prediction problems may require a combination of local and remote predictors.

This deliverable aims to describe indices and data to be used to detect the different types of Extreme Events (EE) considered in CLINT. The extreme events are:

- Tropical cyclones, in terms of genesis and activity on different timescales and extratropical transitions.
- Heatwaves and tropical nights
- Extreme droughts
- Compound events and concurrent extremes

For each type of EE, the report gives an overview of the problem, lists relevant indices and datasets, and discusses candidate drivers.

2 TROPICAL CYCLONES

Tropical Cyclones (TC) form at a rate of about 80-90 times per year globally in the tropical latitude bands on both sides of the Equator. TCs making landfall is among the costliest and deadliest natural disasters. This is due to the strong winds, heavy precipitation, and the associated risk of storm surges. Therefore, it is of paramount importance to be able to accurately predict their activity on several timescales, ranging from a few days to seasonal and climate projections.

A comprehensive theory of TC formation is lacking so far. Several indicators have been developed, however, relating the spatio-temporal distribution of TC formation to large-scale atmospheric and oceanic variables, such as atmospheric humidity, vorticity, and sea surface temperature. These indices generally have good skill at the climatological/global scales at which they have been trained, but their performance tends to degrade at interannual scales, and varies from basin to basin. Another issue with the genesis potential indices is that often their future trends are not consistent with the estimates of future TC activity.
A useful predictor for TC genesis/activity is one that has a reasonable correlation with the target, and shows predictive skill as well. As the predictive skill is different for different predictors, the choice will differ among the different timescales of interest (i.e., a few days ahead vs the climate change time scale). On sub-seasonal timescales, the Madden-Julian Oscillation is a powerful predictor (Klotzbach, 2014) and also possesses predictive skill on a 3-4 week timescale (Vitart, 2009). The open question for the ML design is whether to train on the gridded data that form the indices or directly on the indices.

Within Task 3.1, Subtask 3.1.1 will focus on the long climatological scales, using ML algorithms to discover improved formulations of genesis potential indices based on large-scale climate variables. Subtask 3.1.2, on the other hand, will focus on short time scales, developing ML predictors of TC activity for weather prediction and sub-seasonal time scales.

2.2 Indices for tropical cyclone detection

The Genesis Potential Index (GPI) was developed by Emanuel & Nolan (2004), aiming at describing the climatological distribution and seasonal variations of TCs. Its functional form is given by:

$$GPI \ = |10^5\eta|^{3/2}\left(\frac{H}{50}\right)^3\left(\frac{PI}{70}\right)^3 (1 + \ 0.1\, V)^{-2}$$

where η is the absolute vorticity at 850 hPa, H the relative humidity at 600 hPa, V the wind shear between 200 hPa and 850 hPa and Maximum Potential Intensity (MPI or PI) that is a theoretical estimate of the maximum attainable TC wind speed in a given environment. The calculations behind MPI are described in Emanuel & Bister (2008). MPI values have been computed using the Python package tcpiPY (Gilford 2020)[1].

[1] https://github.com/dgilford/tcpyPI

The Tropical Cyclone Genesis index (TCGI) is an alternative formulation of GPI proposed by Tippett et al. (2011). In the formulation of TCGI, the MPI is replaced by the relative sea surface temperature (SST):

$$TCGI = exp(-4.47 + 0.5\,\eta + 0.05\,H + 0.63\,RSST - 0.17\,V + log\,cos\,\varphi)$$

where η is the absolute vorticity at 850 hPa, H the relative humidity at 700 hPa, V the wind shear between 200 hPa and 850 hPa and RSST is the SST anomaly with respect to the mean tropical SST (30 °N – 30 °S), and φ is the latitude.

Table 1 List of the indices employed in the characterisation and detection of Tropical Cyclones in Task 3.1.

Acronym	Name	Essential climate variables	Description	References
GPI	Genesis Potential Index	vorticity, wind shear, relative humidity, SST	Index describing the spatio-temporal distribution of TC genesis as a function of environmental parameters	Emanuel & Nolan (2004)
TCGI	Tropical Cyclone Genesis Index	vorticity, wind shear, relative humidity, SST	Index describing the spatio-temporal distribution of TC genesis as a function of environmental parameters	Tippett, Camargo & Sobel (2011)
MPI	Maximum Potential Intensity	SST, air temperature, specific humidity, MSLP	Theoretically derived estimate of the maximum intensity attainable by a TC in a given environment	Emanuel (1988), Bister & Emanuel (2008)
ACE	Accumulated Cyclone Energy	wind speed	Lifetime-integral of squared cyclone wind speed	Bell et al (1999)
MJO	Madden-Julian Oscillation	OLR, zonal winds at 850 and 200hPa	2 leading modes of variability in the equatorial region	Hendon and Wheeler, 2004
Nino3.4	Nino3.4	SST	SST anomaly in 5N-5S, 190E-240E,	

***Acronym** = Abbreviation used for the index, **Name** = full name of the index**, Essential climate variables** = variables required for the computation of the index, **Description** = short definition of the index, **References** = Publications where the index is used or defined.*

2.3 Datasets for tropical cyclone detection

Data sets are listed in Deliverable 8.3, 'First update of the Data Management Plan[2]

2.3.1 ERA5

In Subtask 3.1.2, we will use ERA5 as it is a global reanalysis for atmospheric gridded variables. ERA5 is a global ECMWF atmospheric reanalysis available for the period between January 1950 to the present day (Hersbach et al. 2020). It is based on a version of the ECMWF atmospheric model (Integrated Forecasting System, cycle 41r2) that was operational in 2016, and it employs a four-dimensional variational analysis (4D-Var) for data assimilation. ERA5 provides hourly fields with a spatial resolution of approximately 30 km.

As the predictor variables in this task are large scale (see Table 1), we only use the reanalysis data valid 00 UTC for the time-series, and at 2.5-degree resolution, in order to smooth unpredictable noise and to lower the dimensionality for the ML. To generate the training data, ECMWF has created a small software package (CLINT-TS) to create both time series of indices and gridded data for the training. The software and a selection of indices will be available on GitHub.

For the TC genesis indices, ERA5 monthly data from the relevant fields are used, also at a resolution of 2.5 degrees.

In addition to the gridded data from ERA5, we will also use tracking files of TCs from ERA5. This dataset will form an alternative target dataset to IBTrACS. For ERA5, the TCs have been tracked using the tracking algorithm described in Magnusson et al. (2021).

2.3.2 IBTRACS

At least four times a day, each of the Regional Specialized Meteorological Centres (RSMCs) and Tropical Cyclone Warning Centres (TCWCs) produce estimates of the position and intensity of all present TCs in their basin. These observations are often referred to as *Best Track*.

The Best Track is a subjective human assessment of the TC centre's location, intensity, and structure, using all observations available at the time of the analysis. As aircraft missions are generally only present in the Atlantic, the estimates are often based on different satellite products. A common tool is the Dvorak technique (Dvorak, 1984), where the analyst identifies patterns in cloud features in satellite visible and enhanced IR imagery and associates them with an intensity (T) number. From this, look-up tables are available to determine the minimum central pressure (Pmin) and maximum wind speed (Vmax). As this technique involves a human judgment, uncertainties naturally arise both in terms of intensity and whether the system should be classified as a TC or an extratropical one.

After each season, the TCs are re-evaluated, and the estimates can be modified before the final Best Track is completed. The International Best Track Archive for Climate Stewardship (IBTrACS) combines track and intensity estimates from several RSMCs and other agencies to provide a central repository of both working and final Best Track (Knapp et al. 2010).

[2] Table of the Data Management Plan:
https://docs.google.com/spreadsheets/d/1s4igaxwHKxecsrM2ZoQXCbQ_k78B9LpN/edit#gid=2127184400

Table 2 List of observational and reanalysis dataset used in Task 3.1.

Name	Source	Handled by	Processed by	Stored by	ETD	Used by
ERA5	C3S-CDS	CMCC	N/A	ECMWF, CMCC	August 31, 2022	CMCC, ECMWF
IBTrACS		CMCC	N/A	CMCC	August 31, 2022	CMCC, ECMWF

***Name** = short name of the dataset**, Source** = original producer, **Handled by** = partner doing the download/extraction of the dataset over the region of interest, **Processed by** = partner applying any "model output statistics" if any (downscaling, calibration etc.), **Stored by** = partner distributing the data for the consortium partners (e.g., centralised CLINT repository at DKRZ), if need be, **ETD** = estimated date of availability (from handling/storing partner), **Used by** = partner using the data (case study).*

2.3.3 CMIP6 MODEL SIMULATIONS OUTPUT

In order to benchmark the skill of existing genesis potential indices, data at a monthly frequency from a large number of models from the Coupled Model Intercomparison Project Phase 6 (CMIP6) are considered. In particular, simulations output from two model ensembles within CMIP6 are used:

- Scenario Model Intercomparison Project (ScenarioMIP) simulations: this is a large set of GCM simulations covering a number of different climate scenarios. Simulations from the SSP585 (business as usual) and SSP126 (emission stabilisation) are used for the historical (1950-2014) and future (2014-2100) periods. Models in this ensemble have an average horizontal resolution of 1 degree, therefore, direct detection of TCs is not possible.
- High Resolution Model Intercomparison Project (HighResMIP) simulations: this is a smaller set of simulations using high-resolution models, allowing for direct TC detection, and tracking. Simulations from the hist-1950 (1950-2014) and highres-future (2015-2050) simulations are used.

The tracks of the TCs detected in HIGHResMIP simulations were obtained by a public repository, as described in Roberts et al. (2020).

Table 3 List of ScenarioMIP climate projections datasets used in Subtask 3.1.1

Name	Source	Handled by	Processed by	Stored by	ETD	Used by
ACCESS-CM2	ESGF	CMCC	N/A	CMCC	August 31, 2022	CMCC
ACCESS-ESM1-5	ESGF	CMCC	N/A	CMCC	August 31, 2022	CMCC
AWI-CM-1-1-MR	ESGF	CMCC	N/A	CMCC	August 31, 2022	CMCC
BCC-CSM2-MR	ESGF	CMCC	N/A	CMCC	August 31, 2022	CMCC

Name	Source	Handled by	Processed by	Stored by	ETD	Used by
CAMS-CSM1-0	ESGF	CMCC	N/A	CMCC	August 31, 2022	CMCC
CAS-ESM2-0	ESGF	CMCC	N/A	CMCC	August 31, 2022	CMCC
CMCC-CM2-SR5	ESGF	CMCC	N/A	CMCC	August 31, 2022	CMCC
CMCC-ESM2	ESGF	CMCC	N/A	CMCC	August 31, 2022	CMCC
CanESM5	ESGF	CMCC	N/A	CMCC	August 31, 2022	CMCC
EC-Earth3-Veg-LR	ESGF	CMCC	N/A	CMCC	August 31, 2022	CMCC
EC-Earth3-Veg	ESGF	CMCC	N/A	CMCC	August 31, 2022	CMCC
EC-Earth3	ESGF	CMCC	N/A	CMCC	August 31, 2022	CMCC
FGOALS-f3-L	ESGF	CMCC	N/A	CMCC	August 31, 2022	CMCC
FGOALS-g3	ESGF	CMCC	N/A	CMCC	August 31, 2022	CMCC
FIO-ESM-2-0	ESGF	CMCC	N/A	CMCC	August 31, 2022	CMCC
GFDL-ESM4	ESGF	CMCC	N/A	CMCC	August 31, 2022	CMCC
IITM-ESM	ESGF	CMCC	N/A	CMCC	August 31, 2022	CMCC
INM-CM4-8	ESGF	CMCC	N/A	CMCC	August 31, 2022	CMCC
INM-CM5-0	ESGF	CMCC	N/A	CMCC	August 31, 2022	CMCC
IPSL-CM6A-LR	ESGF	CMCC	N/A	CMCC	August 31, 2022	CMCC

Name	Source	Handled by	Processed by	Stored by	ETD	Used by
KIOST-ESM	ESGF	CMCC	N/A	CMCC	August 31, 2022	CMCC
MIROC6	ESGF	CMCC	N/A	CMCC	August 31, 2022	CMCC
MPI-ESM1-2-HR	ESGF	CMCC	N/A	CMCC	August 31, 2022	CMCC
MPI-ESM1-2-LR	ESGF	CMCC	N/A	CMCC	August 31, 2022	CMCC
MRI-ESM2-0	ESGF	CMCC	N/A	CMCC	August 31, 2022	CMCC
NESM3	ESGF	CMCC	N/A	CMCC	August 31, 2022	CMCC
NorESM2-LM	ESGF	CMCC	N/A	CMCC	August 31, 2022	CMCC
NorESM2-MM	ESGF	CMCC	N/A	CMCC	August 31, 2022	CMCC
TaiESM1	ESGF	CMCC	N/A	CMCC	August 31, 2022	CMCC

***Name** = short name of the dataset, **Source** = original producer, **Handled by** = partner doing the download/extraction of the dataset over the region of interest, **Processed by** = partner applying any "model output statistics" if any (downscaling, calibration etc.), **Stored by** = partner distributing the data for the consortium partners (e.g., centralised CLINT repository at DKRZ), if need be, **ETD** = estimated date of availability (from handling/storing partner), **Used by**= partner using the data (case study).*

Table 4 List of HIGHResMIP climate projections datasets used in Task 3.1.

Name	Source	Handled by	Processed by	Stored by	ETD	Used by
CMCC-CM2-SR5	ESGF	CMCC	N/A	CMCC	August 31, 2022	CMCC
CNRM-CM6-1-HR	ESGF	CMCC	N/A	CMCC	August 31, 2022	CMCC
EC-Earth3P-HR	ESGF	CMCC	N/A	CMCC	August 31, 2022	CMCC

Name	Source	Handled by	Processed by	Stored by	ETD	Used by
HadGEM3-GC31-HM	ESGF	CMCC	N/A	CMCC	August 31, 2022	CMCC
MPI-ESM1-2-XR	ESGF	CMCC	N/A	CMCC	August 31, 2022	CMCC

***Name** = short name of the dataset**, Source** = original producer, **Handled by** = partner doing the download/extraction of the dataset over the region of interest, **Processed by** = partner applying any "model output statistics" if any (downscaling, calibration etc.), **Stored by** = partner distributing the data for the consortium partners (e.g., centralised CLINT repository at DKRZ), if need be, **ETD** = estimated date of availability (from handling/storing partner), **Used by**= partner using the data (case study).*

2.3.4 ECMWF FORECAST

In order to benchmark the forecasts based on ML, the ECMWF ensemble forecasting system (ENS) is used. The ensemble system consists of 50 perturbed ensemble members and one unperturbed control member, all using a horizontal resolution of 18 km up to 15 days ahead. The forecasts are run twice a day (00UTC and 12UTC) up to 15 days ahead. Twice a week, the ensemble is extended out to 46 days ahead with 36 km resolution. In each ensemble member, the TCs are tracked (see Magnusson et al. [2021] for tracker description), including cases of genesis during the forecast.
Based on the TC tracks in each ensemble member, a gridded field of probability of TC activity is calculated over a time window. The calculation assumes an impact radius of 300 km. Operationally at ECMWF, the product is calculated with time windows of 2 and 7 days and for the intensity thresholds 8, 17 and 32 m/s. Figure 1 shows examples of the gridded product for tropical storms (>17 m/s) for forecasts valid 17-19 September 2020, initialised on 16 September 00 UTC (left) and 7 September 00 UTC (right). The aim of Subtask 3.1.2 is to produce the same kind of products based on ML.

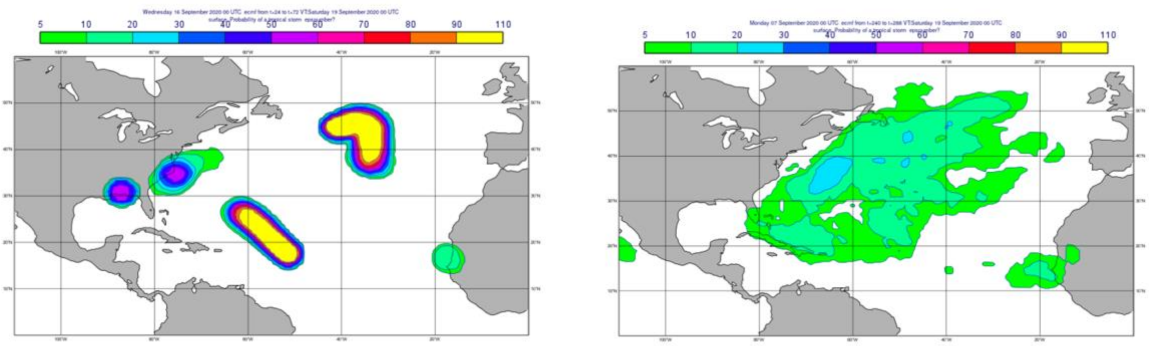

Figure 1 Examples of tropical 2-day storm activity 17-19 September 2020 from ECMWF ensemble with lead time 24-72 hours (left) and 240-288h (right).

2.4 Candidate drivers for tropical cyclones

The aim of Subtask 3.1.2, namely, to define new key structures for TC genesis, requires a comprehensive pool of candidate drivers. Local atmospheric conditions are certainly foremost in terms of the potential for TC genesis over a tropical ocean, as they provide the necessary environmental ingredients. These fields, however, are modulated by different types of tropical waves that imprint their signals onto the local fields. Oceanic conditions determine whether a potential TC can tap the ocean heat content as the vital source to develop and maintain convection-supporting surface heat and moisture fluxes. In addition, certain extratropical conditions are included because TCs occasionally result from interaction with baroclinic structures – a process referred to as 'tropical transition'. These structures are mostly associated with midlatitude dynamics but may also have a tropical history (e.g., tropical upper-tropospheric troughs). Individual candidate atmospheric and oceanic drivers are discussed and motivated in more detail below.

- **Atmospheric drivers:** A variety of studies analysing TC formation (e.g., Palmen 1948, Gray 1968) led to a commonly accepted list of necessary environmental factors. Accordingly, relevant atmospheric factors (and corresponding fields) are the existence of an initial vortex of sufficient strength (850 hPa absolute vorticity), moist mid-to-low levels to foster convection (600 hPa relative humidity), low wind shear (200-850 vertical shear), nonzero Coriolis force, and others. It, therefore, stands to reason that indices for TC genesis, such as the GPI and TCGI introduced above, are defined in a way to combine several of those factors.

  The fields underlying these factors are modulated by different types of tropical waves (Frank and Roundy 2006). A large group of equator-tied waves can be theoretically described by solutions of the shallow water equations (Matsuno 1966), which are referred to as convectively coupled equatorial waves (CCEWs; Kiladis et al. 2009) and include Kelvin, equatorial Rossby, mixed Rossby-gravity and inertio-gravity waves. In contrast, the Madden-Julian Oscillation (MJO) is an empirically discovered wave-like phenomenon that propagates eastward along the Equator. In the North Atlantic, another relevant wave type is the African Easterly wave, which propagates along the off-equatorial African jet, forming 'pouches' frequently conducive to TC formation.

  The MJO is found to have a strong impact on TC genesis in several of the basins, as documented in Klotzbach (2014). For example, over the southern Indian Ocean the TC activity (in terms of accumulated cyclone energy) is, on average, increased by 15-20% during phases 2-5. The role of CCEWs in TC activity has also been demonstrated in various studies both for individual basins and globally (Schreck et al. 2012, Frank and Roundy 2006, Maier-Gerber et al. 2021, Lawton et al. 2022, Schreck et al. 2011). Compared to other models, ECMWF's sub-seasonal forecasts show the lowest biases regarding the mean state and activity of CCEWs and the MJO (Janiga et al. 2018). This confirms the suspected potential of wave indices as predictors for probabilistic forecasts of TC genesis beyond medium-range lead times (Frank and Roundy 2006).

  Although tropical waves are tied to the Equator, they can influence North Atlantic TC formation well outside the Tropics (Schreck et al. 2012, see their Fig. 7). This remote link, along with the fact that tropical waves and TCs are typically nonstationary, makes it difficult to design any local predictors. For Subtask 3.1.2, we will hence test to use the components of the MJO as gridded global fields as training and compare it with training directly on the MJO phases. A common index definition of the MJO is based on the EOFs of OLR, u850 and u200 in the tropical band (Wheeler and Handon, 2004). From the projection onto the two leading EOFs, the phase of the MJO can be determined. If time permits, wave-filtered gridded data are used as input parameters for the ML.

More recent studies have investigated the impact of extratropical processes on subtropical TC activity. Rossby wave breaking (RWB) was found to alter environmental fields (e.g., shear and moisture) in the North Atlantic (Zhang et al. 2016, 2017) and the North Pacific (Wang et al. 2020). Dynamically, this occurs through a potential vorticity (PV) streamer forming at the equatorward side of an anticyclonic RWB event (Thorncroft et al. 1993). Because these structures impact TC activity on (sub-)seasonal timescales (Papin et al. 2020), a candidate driver representing such extratropical influence (e.g., upper-level layer-averaged PV) will be included. Going out to and beyond medium-range lead times, however, PV is not expected to be well forecast by NWP models. Nevertheless, to provide an integrated measure of the baroclinic influence of the upper-level trough, the Coupling Index (CI; Bosart and Lackmann 1995) could be used to represent the bulk tropospheric stability and, thus, the Rossby penetration depth. The CI is calculated as the difference in equivalent potential temperatures at the 2-PVU dynamic tropopause and 850-hPa. Because of its useful application for replacing the canonical SST-based 26.5°C-threshold in case of tropical transitions (McTaggart-Cowan et al. 2015), the CI is considered a relevant extratropical driver. Based on two area-averaged metrics, the upper-level Q-vector convergence (Q) and the lower-level thickness asymmetry (Th), McTaggart-Cowan et al. (2008, 2013) classified five types of baroclinically influenced development pathways for TC genesis. The fields on which the two metrics are based could be another option for PV or CI fields, respectively.

The Quasi-Biennial Oscillation (QBO), a stratospheric driver, has been suggested in the literature as another source to impact Atlantic TC activity (Gray 1984). Its use as a predictor, however, has often been rejected in statistical model development due to weak correlation signals (e.g., Leroy and Wheeler 2008, Henderson and Maloney 2013).

Oceanic drivers: Oceanic conditions are slowly varying and impact the risk of TC genesis and the life length of the systems. Therefore, a candidate driver could be local SSTs over sub-domains of the basins (e.g., the Main Development Region (MDR) or the Gulf of Mexico). Teleconnections, such as the El Niño-Southern Oscillations (ENSO), are believed to influence the large-scale wind patterns remotely over the subtropical Atlantic (Gray 1984) and also the circulation over the Indian Ocean, and thus to impact the TC formation (e.g., Gray 1979, Song et al., 2022). For Subtask 3.1.2, we will test using SST as a gridded global field for training and will compare it with training directly on the ENSO indices and local SST averages.

3 EXTRATROPICAL TRANSITION OF TROPICAL CYCLONES

3.1 Overview

Tropical cyclones (TC) form in the tropics outside the equatorial region. At the end of the life cycle, some TCs curve towards the extratropics and start to interact with the mid-latitudinal flow. Often referred to as Extra-tropical (ET) transitions, these can cause substantial impact in the mid-latitudes, both if the cyclones that directly (Evans et al., 2017; Baker et al., 2021) make landfall in a sub-tropical stage or soon after an extratropical transition (e.g., TC Sandy 2012, TC Leslie 2018, TC Lorenzo 2019) or indirectly (Keller et al., 2019) as the extratropical transitions can lead to downstream development of strong lows (e.g., after TC Karl, 2016; Schäfler et al., 2018). The increased risk of windstorms over Europe originating from ET was investigated by Sainsbury et al. (2020).

Whether or not a TC will approach the extra-tropics is determined by the steering flow in the tropics and the phasing with the mid-latitude wave guide, where an upstream trough favours a northward propagation into the extratropics. Being able to predict the mid-latitudinal flow is, therefore, crucial to capture the ETs.

The majority of TCs do not undergo ET, as they dissipate and/or hit land before reaching higher latitudes. TCs that undergo ET, however, may create substantial impacts downstream over Europe. As was especially evident in 2020, several TCs can make landfall in the deep tropics or subtropics, spinning down quickly into a remnant low-pressure system that can bring substantial flooding rainfall for several days. Other TCs weaken as they encounter high vertical wind shear or substantial low-humidity air, which may occur in the tropics and especially the extratropics. As a TC moves into the extratropics, it also encounters much colder waters, removing the supply of thermal energy and moisture from the ocean that is necessary to maintain the TC.

Figure 2 (top) shows all North Atlantic TCs in the IBTrACS database spanning 1980 to 2021. In this task, we will consider TCs that at least once appeared north of 40°N to be ET cases. Figure 2 (bottom) shows the genesis points of non-ET cases (pink) and ET cases (black). The genesis region might be the first predictor of the risk of ET later in the life cycle.

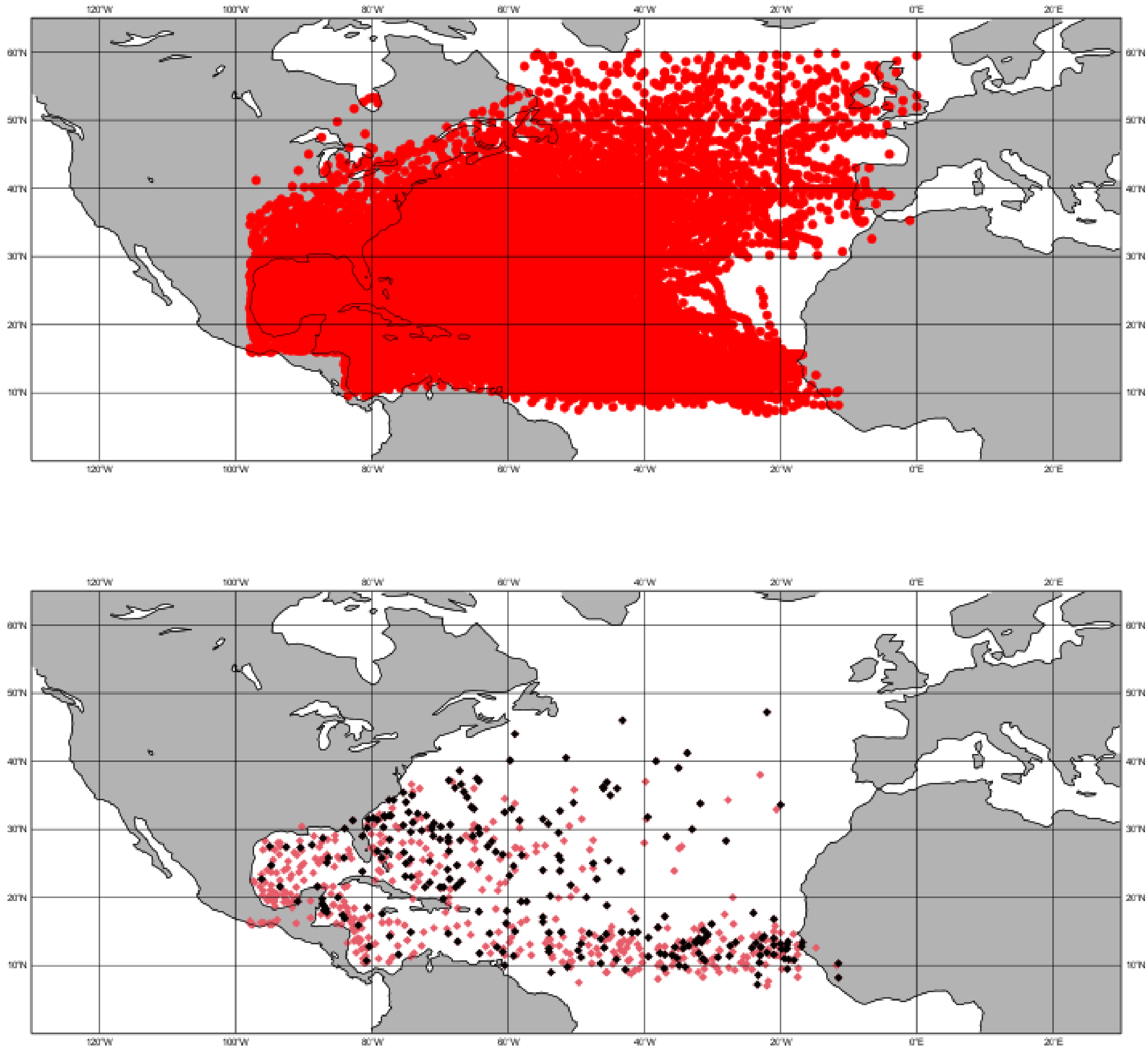

Figure 2 All North Atlantic tropical cyclone positions (top) and genesis points (bottom; non-ET cases - pink, ET cases - black) in the IBTrACS database spanning 1980 to 2021.

Figure 3 shows the inter-annual variability of the fraction of TC undergoing ET. Here we find a large year-to-year variability, which is promising for being able to predict ET if it is possible to identify the predictors responsible for this variability by applying Machine Learning (ML) algorithms. The results will be benchmarked against ECMWF forecasts.

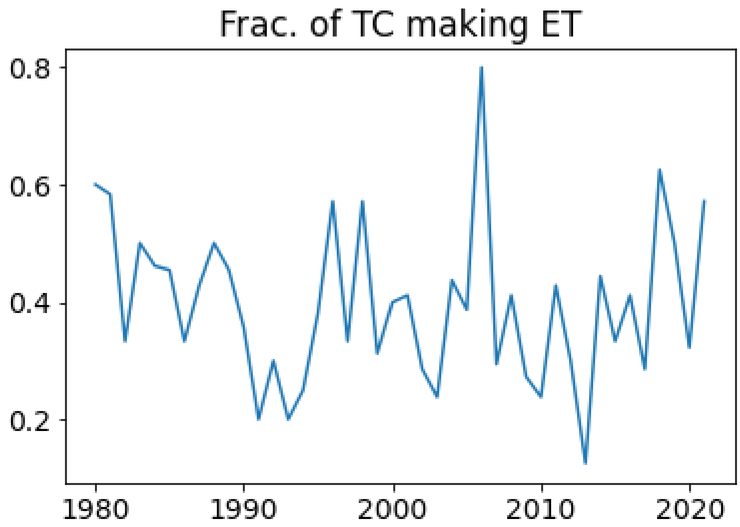

Figure 3 Fraction of TCs undergoing ET each year in IBTrACS 1980-2021.

The aim of this task is to identify candidates for factors influencing the probability of ET of Atlantic TCs, and to create training datasets based on these parameters. While many studies have targeted the processes around ET, we did not find much in the literature on large-scale factors that can be predicted on the timescale 1-2 weeks ahead. The ML problem will be formulated as the conditional probability for ET conditioned on the genesis of TCs.

3.2 Indices for extratropical transition of tropical cyclones

In section 3.1, the candidate drivers for TC genesis (formation point) and activity (integrated track over the life length) are outlined. While these candidates will be important as well for the ET (having a TC is a necessary condition), we introduce here information on the mid-latitude drivers.
In order to create the indices from the ERA5 reanalysis, a software package (CLINT-TS) has been created (to appear on GitHub[3]). Based on the software, a range of indices has been calculated for the period 1980-2022.

[3] https://github.com/climateintelligence

Table 5 List of the indices employed in the characterisation and detection of extratropical transitions in Task 3.1.3.

Acronym	Name	Essential climate variables	Description	References
NAO	North Atlantic Oscillation	z500	The leading mode of atmospheric (z500) variability over the North Atlantic	ECMWF SEAS teleconnection patterns
EAT	East Atlantic Ridge	z500	Mode characterised by an anticyclone over the Central Atlantic	ECMWF SEAS teleconnection patterns
PNA	Pacific-North American	z500	a large-scale weather pattern with two modes, denoted positive and negative, and which relates the atmospheric circulation pattern over the North Pacific Ocean with the one over the North American continent.	ECMWF SEAS teleconnection patterns
NPD	North Pacific Dipole	z500	The second EOF of the Pacific/North American. The sign convention, referred to as the North Pacific dipole, is such that positive projections correspond to an amplification of the respective stationary-wave ridge.	ECMWF SEAS teleconnection patterns
Nino3.4	Nino3.4	SST	SST anomaly in 5N-5S, 190E-240E	
SubAtlSST	Sub-tropical Atlantic SST	SST	SST anomaly in the sub-tropical Atlantic 20N-30N, 60W-20W	

***Acronym** = Abbreviation used for the index, **Name** = full name of the index**, Essential climate variables** = variables required for the computation of the index, **Description** = short definition of the index, **References** = Publications where the index is used or defined.*

3.3 Datasets for extratropical transition of tropical cyclones

3.3.1 ERA5

See 2.3.1.

3.3.2 IBTRACS

See 2.3.2.

Table 6 List of observational and reanalysis datasets used in Task 3.1.3.

Name	Source	Handled by	Processed by	Stored by	ETD	Used by
ERA5	ECMWF MARS	ECMWF	N/A	ECMWF	June 30, 2022	ECMWF
ERA5 TC tracks	ECMWF ECFS	ECMWF		ECMWF	June 30, 2022	ECMWF
IBTrACS	NCEP https://www.ncdc.noaa.gov/ibtracs/	ECMWF		ECMWF	June 30, 2022	
ECMWF ENS TC tracks	ECMWF ECFS	ECMWF		ECMWF	June 30, 2022	ECMWF

Name *= short name of the dataset**, Source** = original producer,* ***Handled by*** *= partner doing the download/extraction of the dataset over the region of interest,* ***Processed by*** *= partner applying any "model output statistics" if any (downscaling, calibration etc.),* ***Stored by*** *= partner distributing the data for the consortium partners (e.g., centralised CLINT repository at DKRZ), if need be,* ***ETD*** *= estimated date of availability (from handling/storing partner),* ***Used by*** *= partner using the data (case study).*

3.3.3 ECMWF forecasts for benchmark

To benchmark the forecasts based on ML, the ECMWF ensemble forecasting system (ENS) will be used. In each ensemble member, the TCs are tracked (see Magnusson et al. (2021) for tracker description), including cases of genesis during the forecast. The forecasts could be verified in a similar method as applied by Bergman et al. (2019), see also 2.3.4.

3.4 Candidate drivers for extratropical transition of tropical cyclones

In the literature, an effort has been made to classify and describe the consecutive stages of a typical ET event (Klein et al. 2000, Jones et al. 2003). Despite the validity of such generalised concepts, several case studies showed that the actual pathway of how ET manifests can vary largely from case to case. This variability results from the complexity of the (thermo)dynamic interplay between the transforming TC, the subtropical high, and the trough embedded in the midlatitude flow. Therefore, the set of predictors used in Task 3.1 comprises candidate drivers for ET of tropical and extratropical origin.

Climatologically, the likelihood of a North Atlantic TC successfully undergoing an ET increases over the season (Bieli et al. 2019). This can be explained by the poleward extending zone of favourable oceanic conditions (i.e., high SSTs) and the equatorward penetrating zone of baroclinic growth associated with the midlatitude dynamics (Hart and Evans 2001). Consequently, a TC would have to cover an increasingly shorter distance through a decay-prone area before reaching the baroclinic influences that induce ET. Different factors contributing to ET cases reaching Europe were investigated by Sainsbury et al. (2022).

With the targeted medium-range lead times, the aim of skilfully forecasting ET requires a combination of the case-specific and the climatological perspectives. While oceanic conditions are slowly varying in general, atmospheric conditions (both tropical and extratropical) range from large-scale patterns to the near-storm environment. Because forecasting ET can be seen as a conditional analysis of TCs, track-related information is considered another major source of predictability. Individual candidate atmospheric, oceanic, and track-related drivers are discussed and motivated in more detail below.

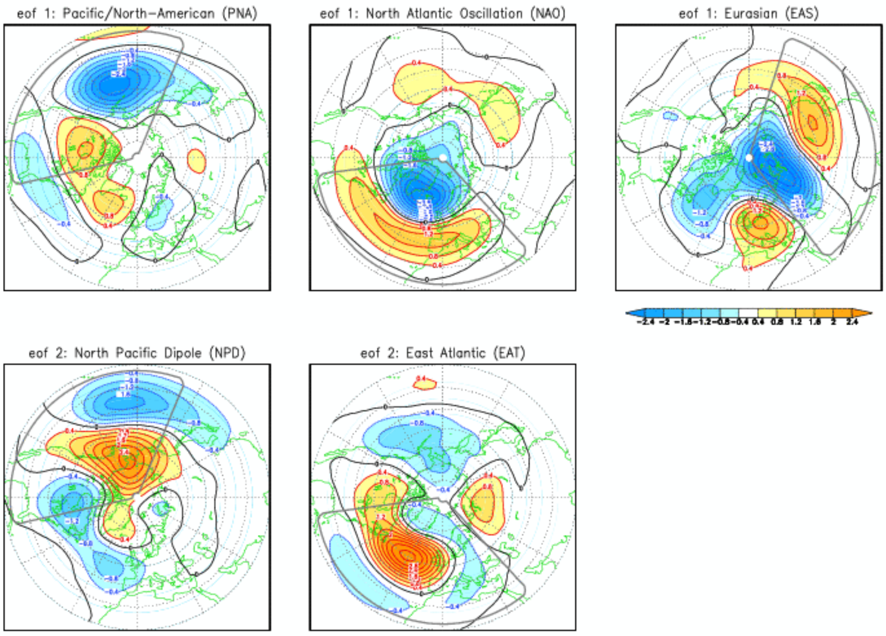

Figure 4 500hPa Teleconnection patterns from ECMWF. (From www.ecmwf.int).

- **Atmospheric drivers:** On the planetary scale, the mid-latitude atmospheric patterns can be diagnosed using an EOF analysis of the 500-hPa geopotential height. In this task we will make use of the teleconnection patterns derived for ECMWF seasonal forecast products. The patterns are based on EOF analysis over two sectors (we will not use the Siberian sector here). Retaining the two leading EOFs, one obtains the Pacific-North American (PNA) and North Pacific Dipole (NPD) from the Pacific sector and North Atlantic Oscillation (NAO) and East Atlantic Ridge (EAT) from the Atlantic sector, respectively. Although NAO and PNA were found to individually explain less than 10% of the year-to-year variability in ET frequency and fraction (Hart and Evans 2001), the indices may be of greater importance for individual ET cases. The Pacific patterns are expected to be relevant for generating the waveguide that later affects the Atlantic, while the Atlantic patterns influence the local conditions for ETs.

On the synoptic scale, idealised simulations have shown that it is not so much the strength of the midlatitude trough (Ritchie and Elsberry 2003) but rather its phasing with the TC that is crucial for ET completion and reintensification (Ritchie and Elsberry 2007). Going out to medium-range lead times, however, the phasing is not expected to be well captured in NWP models. Nevertheless, to provide an integrated measure of the baroclinic influence of the upper-level trough, the coupling index (CI; Bosart and Lackmann 1995) is used for representing the bulk tropospheric stability and, thus, the Rossby penetration depth. The CI is calculated as the difference in equivalent potential temperatures at the 2-PVU dynamic tropopause and 850-hPa. Because of its useful application in an ET case study (McTaggart-Cowan et al. 2003) as well as for replacing the canonical SST-based 26.5 °C-threshold in case of tropical transitions (McTaggart-Cowan et al. 2015), the CI is included as a relevant extratropical driver.

Atmospheric conditions in the near-storm environment are certainly key for the ET process. To first order, most of the variables that enter into the GPI (Emanuel and Nolan 2004) described in MS6-7 should also be relevant to ET, viz. 850-hPa absolute vorticity, 600-hPa relative humidity, and 200-850-hPa vertical wind shear. As those are acting more on a local scale, which is less predictable on the timescale of interest, such quantities could be integrated over regions. The CLINT-TS software is flexible for generating such additional training datasets.

Beyond these conditions of direct physical influence, wave-type tropical drivers, such as the Madden-Julian Oscillation or Convectively Coupled Equatorial Waves, may additionally imprint their signals onto the near-storm environment. As these waves typically are more persistent, they might carry predictive signals from which ET prediction could benefit as well.

- **Oceanic drivers**: Oceanic conditions are slowly varying but climatologically determine the poleward extent of support for the tropical phase, thus setting the pre-ET scene. Relevant drivers for the Atlantic could be local sea-surface temperatures (SST) over sub-domains (e.g., subtropical Atlantic). In Bieli et al. (2020), the predictor selection for the development of an ET prediction model indeed yielded locally averaged SST as one of two key factors. Furthermore, remote influences from teleconnections, such as the El Nino-Southern Oscillation (ENSO), are known to modulate the large-scale wind patterns over the (sub-)tropical Atlantic (Gray 1984). The Southern Oscillation Index (SOI; Troup 1965), a measure for the ENSO state, correlates significantly with ET frequency ($R = +0.228$), as does the NAO index, but has no climatological relationship to ET fractions in the North Atlantic (Hart and Evans 2001). However, it may be that in individual cases, there is a more direct connection with ENSO.

- **Track-related drivers:** In addition to the atmospheric and oceanic drivers, track-related information is deemed to be particularly relevant for ET prediction. Beside the apparent geographical differences in genesis locations (LATgen, LONgen) between ET and non-ET cases discussed in Hart and Evans (2001) and displayed in Figure 2, a recent study by Datt et al. (2022) showed that the degree of baroclinic influence during TC genesis impacts on whether the TC eventually undergoes ET. This suggests that there is some sort of 'memory' effect that can be exploited for ET prediction. The underlying development pathways were proposed by McTaggart-Cowan et al. (2008, 2013) based on two area-averaged metrics: the upper-level Q-vector convergence (Q) and the lower-level thickness asymmetry (Th). In the North Atlantic, the strong tropical transition and trough induced pathways are significantly more likely to result in ET than the other pathways (Datt et al. 2022). Since this relationship still holds when controlling for genesis latitude, the demonstrated relationship to ET fraction gives rise to consider these metrics in our models, either directly as drivers or by training models separately for individual pathways.

Along with information on track history, predictors representing the TC's current state will be provided to the model. Basic track-related predictors are included for cyclone position (LAT, LON), intensity (central pressure, max. sustained wind), and movement (heading angle, translation speed). Although Bieli et al. (2020) identified latitude as the only relevant track-related predictor for their ET prediction model, we nevertheless include all the aforementioned in our predictor pool to ensure that a comprehensive set is provided.

Cyclone phase space (CPS; Hart 2003) metrics, nowadays widely accepted in the operational and research communities, give insight into a cyclone's thermal symmetry (B metric), upper-level thermal wind (-VTU metric), and lower-level thermal wind (-VTL metric). Analysing a cyclone's trajectory in CPS allows it to identify phase transitions (e.g., ET). During a North Atlantic ET, the TC usually first acquires a cold core before losing its symmetric thermal structure, which is the reverse of the usual global behaviour (Bieli et al 2019). Despite its utility and acceptance, the CPS concept was shown to predict North Atlantic ET worse compared to a simple logistic regression model (Bieli et al. 2020), which motivates its use as for candidate drivers but also to better leave the prediction component to a dedicated (statistical) model.

4 HEATWAVES AND TROPICAL NIGHTS

4.1 Overview

Heat waves (HW) and tropical nights (TN) are among the most frequent extreme climate events that cause immense stress on human health and ecosystems, but also socio-economic losses when affecting agriculture or energy systems (Thomas et al. 2020; García-Martínez et al. 2021). The relationship between heat waves and mortality has already been demonstrated for specific episodes (see Perkins et al. 2015 and references therein), however, the impact of above-normal night-time temperatures should not be neglected, as it has significant effects on human health (Trigo et al., 2005). Other reported HW impacts include increased electricity demand and decreased power production (Zuo et al., 2015), heat stress on vegetation activity and terrestrial ecosystems, as well as increasing risk of wildfires, droughts and crop yields (e.g., Lesk et al., 2016).

HWs can occur in combination with other hazards, therefore conforming compound events. Examples of HW-compounded hazards include high humidity (humid HWs; e.g., Russo et al., 2017) or droughts (e.g., Miralles et al., 2014). For example, the combination of abnormally high night-time temperatures with increased humidity can lead to reduced body regeneration, attenuated thermoregulation, exhaustion, and other physiological effects favouring increased morbidity and premature deaths (Scoccimarro et al. 2017, Kendrovski et al. 2017). Hence, the detection of those EE in advance might be crucial for the development of prevention plans, and mitigation strategies that can minimise the risks associated with both HW and TN events.

For the detection of HW and TN, it is important to understand the mechanisms that trigger and maintain the events. HWs result from large- and smaller-scale processes, including the atmospheric circulation and anomalous regional conditions in slowly varying components, such as land-surface, SST or sea ice (e.g., Sillmann et al., 2017; Coumou et al., 2018 and references therein). These regional conditions can be modulated by internal modes of variability and changes in external forcings (Perkins, 2015). In particular, several studies have shown that heat waves are mainly related to persistent high-pressure systems (Matsueda et al. 2011, White et al. 2021), and they are linked to specific soil moisture conditions (Seneviratne et al. 2006; Alexander et al. 2010). The mechanisms behind the tropical nights have been less discussed, but the atmospheric conditions, together with air humidity and cloud cover, have been suggested as the main drivers of these EE (Thomas et al. 2020; Luo et al. 2022).

This section describes the indices used for HW and TN detection and the datasets and drivers that will be employed in Task 3.2 on the use of Artificial Intelligence (AI) and Machine Learning (ML) techniques to detect HW and TN. The ML algorithms will be used to select the candidate drivers of both HW and TN and to link these drivers with the EE over Europe.

4.2 Indices for heatwaves and tropical nights detection

The characterisation of extreme events is usually performed by employing specific indices. These indices are particularly useful to quantify the severity, magnitude and duration of the EE compared to other episodes. In task 3.2, several indices (Table 7) have been employed to ensure that the detection of heat waves and warm nights is performed in a comprehensive way.
One of the indices used for the evaluation of the heat waves and the corresponding index for the tropical nights (HWMI and TNMI, respectively) are illustrated in Figure 5 for the summer (2022). These indices provide similar information, but they allow us to investigate different aspects of extreme temperature conditions.
The applicability to specific agriculture or water sectors has been considered (https://climpact-sci.org/), and these indices have been assessed by the Expert Team on Sector-specific Climate Indices (ETSCI, https://www.wmo.int/pages/prog/wcp/ccl/opace/opace4/ET-SCI-4-1.php). Technical details involved in their computation follow the recommendations of Crespi et al. (2020).

Table 7 List of the indices employed in the characterisation and detection of the heat waves and warm nights in Task 3.2.

Acronym	Name	Essential climate variables	Description	References
HWMI	Heat Wave Magnitude Index	Tmax (daily maximum temperature)	The maximum heat wave magnitude represents the strongest heatwave for a given	Russo et al. (2014); Prodhomme et al. (2021)

Acronym	Name	Essential climate variables	Description	References
			season in terms of both duration and intensity.	
TNMI	Tropical Night Magnitude Index	T2M (2-meter temperature, Sea level pressure, dewpoint	The maximum tropical night magnitude that represents the strongest tropical night period (i.e., consecutive days with warm night conditions) for a given season in terms of both duration and intensity.	Russo et al. (2017); Torralba et al. (in preparation)
Tmax_ NBDAYSQ90	Number of days with Tmax above the 90th percentile	Tmax	The number of daily maximum temperatures exceeding the smoothed 90th percentile within the considered season (15MJJA).	Prodhomme et al. (2021)
Tnight_ NBDAYSQ90	Number of days with Tnight above the 90th percentile	T2M, Sea level pressure, dewpoint	The number of days with the average temperature at night (between 23-06 local time) exceeding the smoothed 90th percentile within the considered season (15MJJA).	Torralba et al. (in preparation)
HMD	Heat Magnitude Day	Tmax (daily maximum 2-meters temperature)	Accumulates heat wave magnitude (as in Russo et al. 2015) for the 3-month period before the harvesting season, representing heat stress within this period.	Zampieri et al. (2017), Toreti et al. (2019a)
HWS	Heat Wave Severity	Tmax or Tmin (daily maximum/minimum 2-meters temperature)	Accumulated temperature exceedance (above the local 90th percentile) for all heat wave days (temperature exceeding the 90th percentile) over a user-defined interval (monthly, seasonal, etc.)	Perkins-Kirkpatrick & Lewis (2020)
ECATR	Tropical nights index per time period	Tmin (daily minimum temperature)	The number of tropical nights when the daily minimum temperature exceeds a temperature threshold	ECATR
ECAHWDI	Heat wave	Tmax (daily	The	http://etccdi.pacificcli

Acronym	Name	Essential climate variables	Description	References
	duration index	maximum temperature), TXnorm (the mean of Tmax of a given climate reference period)	number of days with heat waves with respect to mean reference period	mate.org/indices.shtml

***Acronym** = Abbreviation used for the index, **Name** = full name of the index**, Essential climate variables** = variables required for the computation of the index, **Description** = short definition of the index, **References** = Publications where the index is used or defined.*

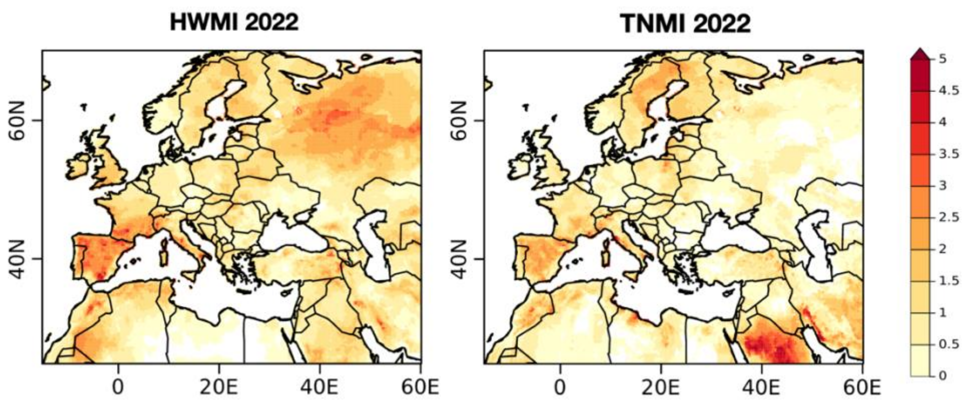

Figure 5 Heat Wave Magnitude index (HWMI, left panel) and Tropical Night Magnitude index (TNMI, right panel) for the extended summer of 2022. These indices have been computed with the ERA5 daily data (from the 15th of May to the 31st of August).

4.3 Datasets for heatwaves and tropical nights detection

4.3.1 ERA5

In task 3.2, we will use ERA5 as it is a global reanalysis for the HW and TN detection. See 2.3.1.

4.3.2 ERA 20C

ERA 20C is ECMWF's first atmospheric reanalysis of the 20th century, from 1900 to 2010. It assimilates observations of surface pressure and surface marine winds only (Poli et al 2016). ERA-20C was produced with IFS version Cy38r1. A coupled Atmosphere/Land-surface/Ocean-waves model is used to reanalyse the weather by assimilating surface observations, utilising a 4D-Var data assimilation scheme that is comparable to numerical weather prediction, assimilating surface winds over the ocean in addition to surface pressure over ocean and land, with variational bias correction of surface pressure observations. The ERA-20C products describe the spatio-temporal evolution of the atmosphere (on 91 levels in the vertical, between the surface and 0.01 hPa), the land surface (on 4 soil layers), and the ocean waves (on 25 frequencies and 12 directions). The assimilation methodology is a 24-hour 4D-Var analysis, with variational bias correction of surface pressure observations. The temporal resolution of the daily products is 3 hours. The horizontal resolution is approximately 125 km (spectral truncation T159).

4.3.3 20CRv3

The NOAA-CIRES-DOE Twentieth Century Reanalysis version 3 (20CRV3) is a reanalysis dataset providing data for the period 1836/01/01 to 2015/12/31 at 3-hourly frequency (Silvinski et al 2019). 20CRv3 is run at a resolution of T254 (approximately 75 km at the Equator) with 64 vertical levels up to .3mb and 80 individual ensemble members. The surface pressure observations have been made available through international cooperation facilitated by the Atmospheric Circulation Reconstructions over the Earth (ACRE) initiative and working groups of the Global Climate Observing System (GCOS) and World Climate Research Programme (WCRP).

Table 8 List of observational and reanalysis dataset used in Task 3.2.

Name	Source	Handled by	Processed by	Stored by	ETD	Used by
ERA5	C3S-CDS	CMCC	N/A	CMCC	June 30, 2022	CMCC, JLU
ERA20C	C3S-CDS	CMCC	N/A	CMCC	June 30, 2022	CMCC, JLU
20CRv3	NOAA	CMCC	N/A	CMCC	June 30, 2022	CMCC, JLU

***Name** = short name of the dataset**, Source** = original producer, **Handled by** = partner doing the download/extraction of the dataset over the region of interest, **Processed by** = partner applying any "model output statistics" if any (downscaling, calibration etc.), **Stored by** = partner distributing the data for the consortium partners (e.g., centralised CLINT repository at DKRZ), if need be, **ETD** = estimated date of availability (from handling/storing partner), **Used by** = partner using the data (case study).*

4.3.4 CMIP6 model simulations

The sample of extreme events available for the training of ML algorithms will be augmented by training the algorithms also on climate model data in addition to the reanalysis products. While GCMs simulations are affected by biases, their use provides the advantage of being able to rely on several hundred or even thousands of years of simulated climate data. Appropriate techniques will be put in place to ensure the use of modelled data does not degrade the accuracy of the trained ML algorithms. As an example, the algorithms could be trained at first on the model data and then re-trained on observations/ reanalysis data via transfer learning techniques (Asch et al. 2022, Jacques-Dumas et al. 2021).
In this context, CMIP6 climate model simulations will be used to enlarge the input data for the training of the ML methods (pre-industrial control runs and/or ensembles of historical simulations). Among all the models contributing to the CMIP6 ensemble, two models have been initially selected

for testing and evaluation of ML algorithms: CMCC-CM-SR5 and MPI-ESM-MR. Those models are based on two different dynamical cores and are therefore expected not to share similar biases among them. This list can be expanded during the project by including other standard CMIP6 model simulations available at CDS if, during the development of Machine Learning algorithms, it is found that a larger training set is needed.

Table 9 List of climate projections datasets used in Task 3.2.

Name	Source	Handled by	Processed by	Stored by	ETD	Used by
CMCC-CM2-SR5	CMCC	CMCC	N/A	CMCC	June 30, 2022	CMCC, Hereon
MPI-ESM-MR	Hereon	Hereon	Hereon	DKRZ	June 30, 2022	CMCC, Hereon

Name *= short name of the dataset, Source = original producer,* ***Handled by*** *= partner doing the download/extraction of the dataset over the region of interest,* ***Processed by*** *= partner applying any "model output statistics" if any (downscaling, calibration etc.),* ***Stored by*** *= partner distributing the data for the consortium partners (e.g., centralised CLINT repository at DKRZ), if need be,* ***ETD*** *= estimated date of availability (from handling/storing partner),* ***Used by****= partner using the data (case study).*

4.3.5 C3S seasonal forecasts

The current capabilities of the seasonal prediction systems to predict HW and TN have been explored in the multi-system framework provided by the Copernicus Climate Change Service (C3S) initiative. The ability of the C3S seasonal forecast systems to detect those EE at seasonal timescales will be used as a benchmark to quantify the potential added value of the ML methods developed in Task 3.2. Particularly the C3S seasonal forecasts produced by different institutions will be employed: ECMWF (European Centre for Medium-Range Weather Forecasts), DWD, Météo-France and CMCC (Centro Euro-Mediterraneo sui Cambiamenti Climatici). The main specifications of these prediction systems are listed in Table 10, but all the systems provide 6-hourly fields spanning six months into the future, with a spatial resolution of 1° and global coverage. The number of ensemble members (i.e., the different realisations used to sample the seasonal forecast uncertainty) varies among the different seasonal forecast systems (See Table 10).

Table 10 List of seasonal forecast datasets used in Task 3.2.

Name	Source	Handled by	Processed by	Stored by	ETD	Used by
Meteo France System 7	C3S-CDS	CMCC	N/A	CMCC	June 30, 2022	CMCC
DWD System 2.1	C3S-CDS	CMCC	N/A	CMCC	June 30, 2022	CMCC

Name	Source	Handled by	Processed by	Stored by	ETD	Used by
CMCC SPS3.5	C3S-CDS	CMCC	N/A	CMCC	June 30, 2022	CMCC
ECMWF SEAS5	C3S-CDS	CMCC	N/A	CMCC	June 30, 2022	CMCC

An example of the current level of forecast quality in the seasonal predictions of the HW and TN indices is shown in Figure 6. The CMCC SPS3.5 has high correlation values for both the HWMI and the TNMI in southern Europe for the extended summer season. However, low correlation values are obtained in northern Europe.

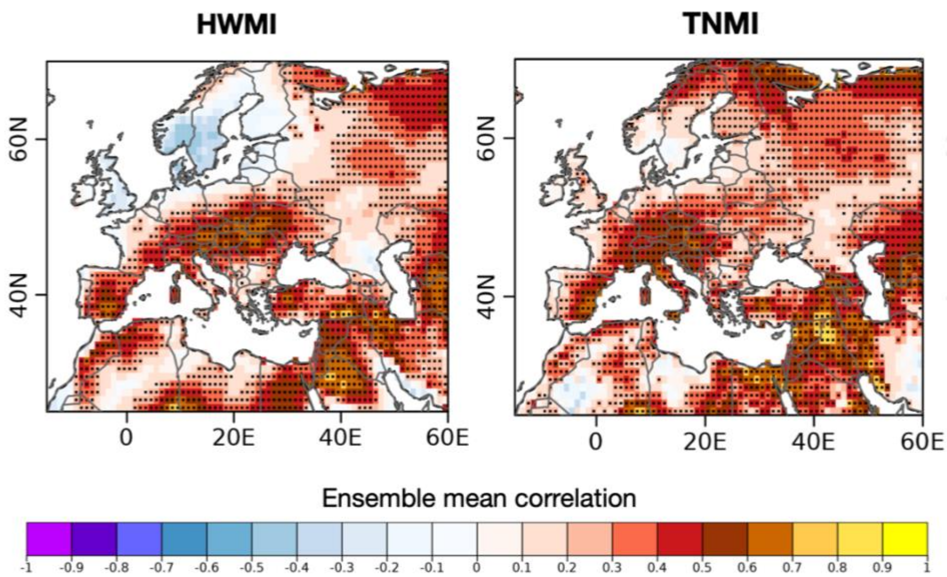

Figure 6 Ensemble mean correlation of the CMCC SPS3.5 seasonal prediction system for Heat Wave Magnitude index (HWMI, left panel) and Tropical Night Magnitude index (TNMI, right panel) in the 1993-2016 period and in the 15MJJA season. The seasonal forecasts were issued on the 1st of May and the observational reference is ERA5.

4.4 Candidate drivers for heatwaves and tropical nights

The mechanisms leading to daytime HW are usually associated with high-pressure atmospheric systems (e.g., blocking, circum-global teleconnection patterns), which favour warm horizontal advection, subsidence and diabatic heating (e.g., enhanced shortwave radiation and sensible heating (Sousa et al. 2018). However, TNs are most likely linked to increased cloud cover, humidity, downward longwave radiation and/or low-level temperature advection (Thomas et al. 2020; Luo et al. 2022). These differences in the processes involved in the occurrence of the two types of EE might suggest that different drivers might be required for the ML methods to effectively detect both HW and TN.

Based on the literature, the following regional and large-scale phenomena are considered as potential drivers of European heatwaves and warm nights:

- **Atmospheric conditions:** The involved atmospheric patterns can be diagnosed using 500-hPa geopotential height and/or sea level pressure fields (Lau and Nath 2012; Loikith and Broccoli 2012). The most relevant teleconnection patterns linked to heat waves have been the North Atlantic Oscillation (NAO, Kenyon and Hegerl 2008) or the atmospheric Blocking (e.g., Matsueda 2011; Schaller et al., 2018, Kornhuber et al., 2019). Favourable heat wave conditions can be triggered by tropical-extratropical teleconnections forced by intraseasonal variations in tropical convection (e.g., the Madden-Julian Oscillation, MJO; Cassou et al. 2005). Although atmospheric circulation largely determines the key physical processes (e.g., temperature advection, radiative fluxes), other atmospheric fields can help constraining regional conditions and the severity of the event (e.g., humidity; Thomas et al. 2020; Luo et al. 2022).

- **Slowly varying factors**: They account for boundary conditions in other components of the climate system that promote interactions and/or feedbacks with the atmosphere, potentially amplifying the severity of the event. In particular, the HN and TN links have been suggested with the following:

    - Ocean: North Atlantic sea surface temperatures (SSTs) (Cassou et al. 2005; Duchez et al. 2016), The El Niño–Southern Oscillation (ENSO) (Zhu et al. 2015; Wulff et al. 2017), Atlantic Multi-decadal Oscillation (AMO) (Della-Marta et al. 2007), Pacific Decadal Oscillation (PDO) (Kenyon and Hegerl 2008).

    - Land: Regional and/or remote soil moisture deficit, surface heat fluxes, warm horizontal advection (Quesada et al. 2012, Miralles et al. 2019; Ardilouze et al. 2019; Materia et al. 2021).

    - Sea-ice: Arctic sea-ice extent (Coumou et al. 2018)

5 EXTREME DROUGHTS

5.1 Overview

Drought is a natural phenomenon mostly related to the reduction in the amount of precipitation received over an extended period, such as a season or a year (Mishra and Singh, 2010). In contrast to aridity, drought is not permanent, although prolonged droughts may propagate through the full hydrological cycle, resulting in significant long-term economic, social, and environmental costs (Spinoni et al., 2016). In the context of current global climate change, characterised by rising temperatures and more extreme precipitation regimes, drought is considered one of the most relevant natural disasters, and there is a consensus that the situation will get worse in the coming decades (Spinoni et al., 2018).
Despite drought being a hot topic extensively studied in the literature, there is still no unanimity on its definition. Some common definitions of the concept, adapted to the discipline or the sector they

refer to, are given by (i) The World Meteorological Organization (WMO, 1986), which states "drought means a sustained, extended deficiency in precipitation"; (ii) The Food and Agriculture Organization (FAO, 1983) of the United Nations that defines a drought hazard as "the percentage of years when crops fail from the lack of moisture"; (iii) Palmer (1965) who described a "drought as a significant deviation from the normal hydrological conditions of an area". These definitions clearly differ for the variables used to define it, namely precipitation, crop yield, and streamflow, and they refer to different stages of the development of drought. As a matter of fact, drought is a phenomenon that evolves at multiple scales (Vicente-Serrano et al., 2010). The period from the arrival of water inputs (as rainfall, snow, river discharges, etc.) to the availability of a given usable resource may vary considerably. As a consequence, the time horizon over which the water deficit is considered becomes of key importance.
Depending on the time horizon considered and the hydro-climatic variable used in drought characterisation, droughts are generally classified into three categories (Pedro-Monzonís et al., 2015):

1. A meteorological drought is defined as a lack of precipitation over a region for a period of time. Since a meteorological drought is the primary cause of a drought, while the other types describe secondary effects on specific economic compartments, it is often regarded as the key type of drought (Spinoni et al., 2016).
2. An agricultural drought may be defined as a moisture deficit in the root zone affecting crop development and declining crop yields. This type of drought, triggered by a meteorological one, usually develops in the medium term (3-6 months).
3. A hydrological drought refers to a lack of water in the hydrological system, manifesting itself in abnormally low streamflow in rivers and abnormally low levels in lakes, reservoirs, and groundwater. Hydrological droughts, which occur after several months of low precipitation and deficient soil moisture, can cover extensive areas and last for months to years.

There is also another approach to drought analysis, namely through the concept of operational drought, which refers to a period with supply anomalies. A dry period may, in fact, be caused by a lack of water resources or, especially in highly regulated contexts, an exceedance of demand due to inadequate management of the water exploitation system (Pedro-Monzonís et al., 2015). An operational (or socio-economic) drought is associated with the condition of Water Scarcity, defined as a situation where insufficient water resources are available to satisfy long-term average requirements and, similarly, impacts that can manifest months or years after the event ends.
This chapter report describes the traditional indices used for drought detection, along with the datasets that will be used in Task 3.3 for the computation of such indices at the European scale as well as in the CLINT Climate Change Hotspots. Lastly, the report includes a preliminary set of candidate drivers for drought detection and prediction that will be processed by the Machine Learning algorithms developed in WP2 to design Artificial Intelligence-enhanced drought indices.

5.2 Indices for drought detection

Drought indices are quantitative measures that characterise drought in terms of intensity, onset, termination, duration, and severity by assimilating data from one or several variables into a single numerical value. Operationally, drought indices can be applied for drought detection and real-time monitoring, drought evaluation, correlation of drought severity with drought impacts, drought

forecasting, and, finally, allowing the declaration of drought levels which instigate drought risk management measures (Zargar et al., 2011).
Just as there is no single definition of drought, no single index can account for and be applied to all types of droughts, climate regimes, and sectors affected (Svoboda et al., 2016). More than 150 drought indices have been developed by several generations of researchers during the 20th century (Zargar et al., 2011). The selection of an appropriate drought index must be driven by the suitability of the index for the considered drought type; data availability; temporal and spatial scale of the analysis; statistical consistency (Steinemann et al., 2005). Therefore, we distinguish the indices that will be used for detecting droughts at the European scale (Table 11) from those locally adopted in the CLINT Climate Change Hotspots (Table 12). The latter have been identified from the direct interactions with the local end-users (for details, see Deliverable D6.1 - Local Climate Services).
CLINT aims at advancing traditional drought detection by defining AI-enhanced, impact-based drought indices that link the observed impacts of extreme droughts (e.g., reduction of electricity production or crop failures) with the candidate drivers of the event, including climatic, meteorological and hydrological variables over different spatial and temporal scales.

Table 11 List of the indices for drought detection at the European scale.

Acronym	Name	Essential climate variables	Description	References
SPI	Standardised Precipitation Index	Precipitation	SPI represents the number of standard deviations the cumulative precipitation deviates from the average of a standardised normal distribution.	Hayes et al. (1999); McKee et al. (1993)
SPEI	Standardised Precipitation and Evapotranspiration Index	Precipitation and Potential Evapotranspiration (Temperature)	Similar to SPI, SPEI represents the deviations from the average of a standardised distribution but replaces the precipitation data with the difference between precipitation and potential evapotranspiration. SPEI tends to be more effective than SPI in arid climates, where evapotranspiration has a key role in depleting soil moisture.	Beguería et al. (2010); Vicente-Serrano et al. (2010)
SRI	Standardised Runoff Index	Streamflow	Similar to SPI, SRI represents the deviations from the average of a standardised distribution but replaces the precipitation data with the streamflow ones. SRI aims to capture the hydrologic processes	Shukla and Wood (2008); Vicente-Serrano et al. (2011)

Acronym	Name	Essential climate variables	Description	References
			that determine seasonal lags in the influence of climate on streamflow.	
SSI	Standardised Soil moisture Index	Soil moisture	Similar to SPI, SSI represents the deviations from the average of a standardised distribution but replaces the precipitation data with the soil moisture ones. Compared to SPI, SSI generally indicates a more reliable drought persistence, while it is less effective in capturing drought onset	Hao and Aghakouchak (2013),

Table 12 List of the indices for drought detection in the CLINT Climate Change Hotspots.

Hotspot	Name	Essential climate variables	Description
Zambezi Watercourse	Low streamflow	Streamflow	The Zambezi Watercourse Commission detects extreme droughts by looking at low-water levels in rivers and lakes impacting irrigated agriculture and hydropower generation.
Douro River Basin	Prolonged drought index; scarcity index	Streamflow and Precipitation; reservoir levels and supply deficits in socioeconomic demands	The Douro River Basin Authority detects prolonged droughts by looking at precipitation deficits and low-water levels in rivers and scarcity situations by estimating the different levels of supply deficits in irrigated agriculture based on the near-real-time reservoir levels.
Rijnland	Standardized Precipitation Index, Precipitation deficit, Low streamflow	Precipitation, Evapotranspiration, Streamflow	Rijnland water board detects drought events by looking at precipitation deficit in the catchment and at Rhine discharges at Lobith, where the Rhine enters the Netherlands.
Aa en Maas	Low groundwate	Groundwater level and discharge	Aa and Maas water board detects drought events by looking at precipitation deficit in the

Hotspot	Name	Essential climate variables	Description
	r levels and discharge		catchment, groundwater tables and Muese discharges.
Lake Como Basin	Low lake inflow	Streamflow	Consorzio dell'Adda (i.e., the institutional operator of Lake Como) detects extreme droughts when the monthly net inflows to the lake are lower than the tenth percentile of historical values.

5.2.1 European droughts

Droughts at the European scale are detected by using standardised indices (see Table 11). The Standardised Precipitation Index at a 1-month accumulation period (SPI-1, see top row of Figure 7) is often used for the detection of meteorological droughts, the Standardised Precipitation and Evapotranspiration Index at 3-month accumulation period (SPEI-3, see the middle row of Figure 7) for agricultural droughts, and the Standardised Runoff Index at 6-month accumulation period (SRI-6, see the bottom row in Figure 7) for hydrological droughts. These indices are computed using data from HydroGFD2.0 and E-HYPE model simulations (see next section) over the time period 1993-2018.

The analysis of drought occurrence (left column of Figure 7) shows that the regions that experienced the highest number of drought events are Southern England, Northern France, and Northern Italy, along with Southern Spain and Ukraine but only in terms of SPEI-3. In terms of drought duration (right column of Figure 7), the areas that experienced the longest droughts of any accumulation period are instead the Baltic Sea region, Normandy, and Southern Italy.

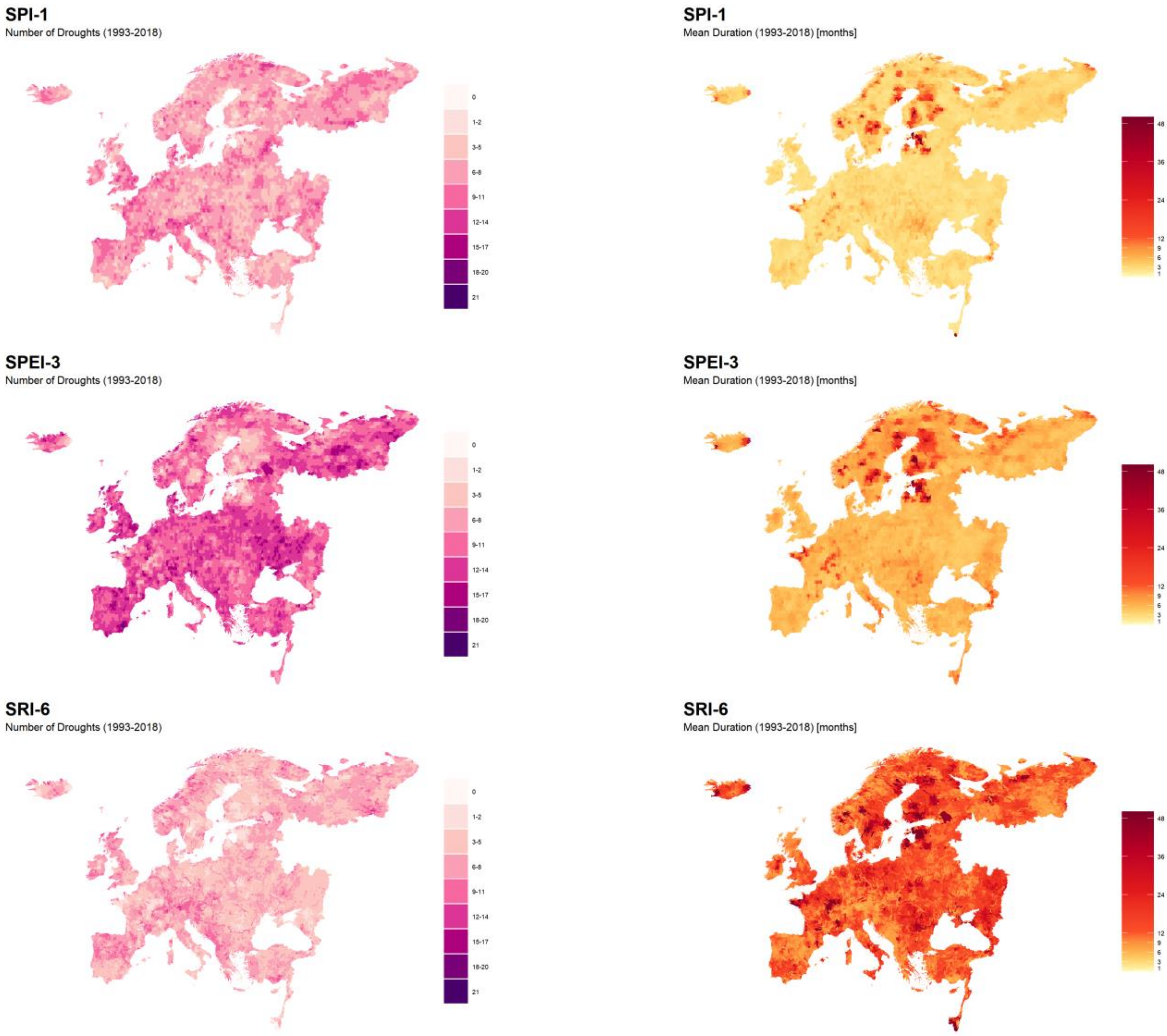

Figure 7 Occurrence (left column) and mean duration (right column) of drought events at the European scale. The top row shows the SPI-1 (1-month accumulation period), the middle row the SPEI-3 (3-month accumulation period), and the bottom row the SRI-6 (6-month accumulation period).

5.2.2 Zambezi watercourse

The Zambezi Watercourse Commission monitors drought events by looking at low-water levels in rivers and lakes. Given the availability of streamflow observations for the main four sub-basins of the watercourse, namely Upper Zambezi (Victoria Falls station), Kafue River (Kafue Hook Bridge station), Luangwa River (Great East Road Bridge station), and Shire River (Mangochi station) that were collected during the DAFNE research project (http://dafne-project.eu/), and the lack of observed levels in water reservoirs considered sensitive data collected by hydropower companies, we detect historical droughts when the monthly streamflow data are below the 25th percentile of the historical observations in that month.

The top panel of Figure 8 illustrates the trajectory of monthly streamflow for the Upper Zambezi over the period 1986-2005. The middle panel shows the anomaly of the flow with respect to the 25th percentile thresholds, with the negative values (red) identifying drought events. The lower the value, the more intense the drought event. Lastly, the bottom panel shows the occurrence of drought events that are represented by vertical lines, where thick lines mark long events.
The results in Figure 8 show the summers of 1992-1994-1995-1996 as the most intense drought events, with the period 1994-1996 representing a prolonged, multi-annual drought event. These findings confirm the data reported in ZAMCON (2015).

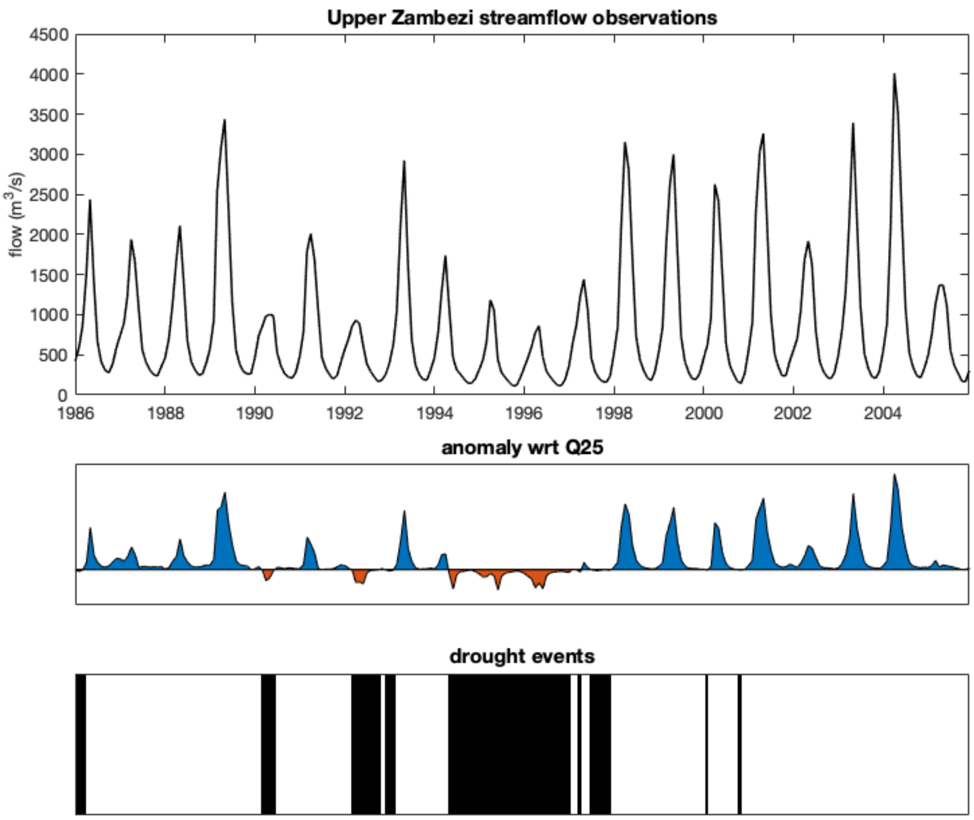

Figure 8 Drought events in Upper Zambezi River (Victoria Falls station) according to the definition adopted by the Zambezi Watercourse Commission. Top: monthly historical observations; Middle: anomaly of monthly flow with respect to the 25th percentile (Q25) of the historical values in the same month; Bottom: occurrence of drought events.

Figure 9 compares the streamflow data in the four sub-basins (top panel) and the corresponding occurrence of drought events (bottom panel). Results show that the Upper Zambezi and Kafue Rivers tend to have registered similar drought events, likely because of their spatial proximity. The droughts detected on the Shire River exhibit some differences but confirmed the multi-annual event between 1992 and 1996. Conversely, the droughts detected on the Luangwa River have a more diverse pattern, with shorter and more frequent events.

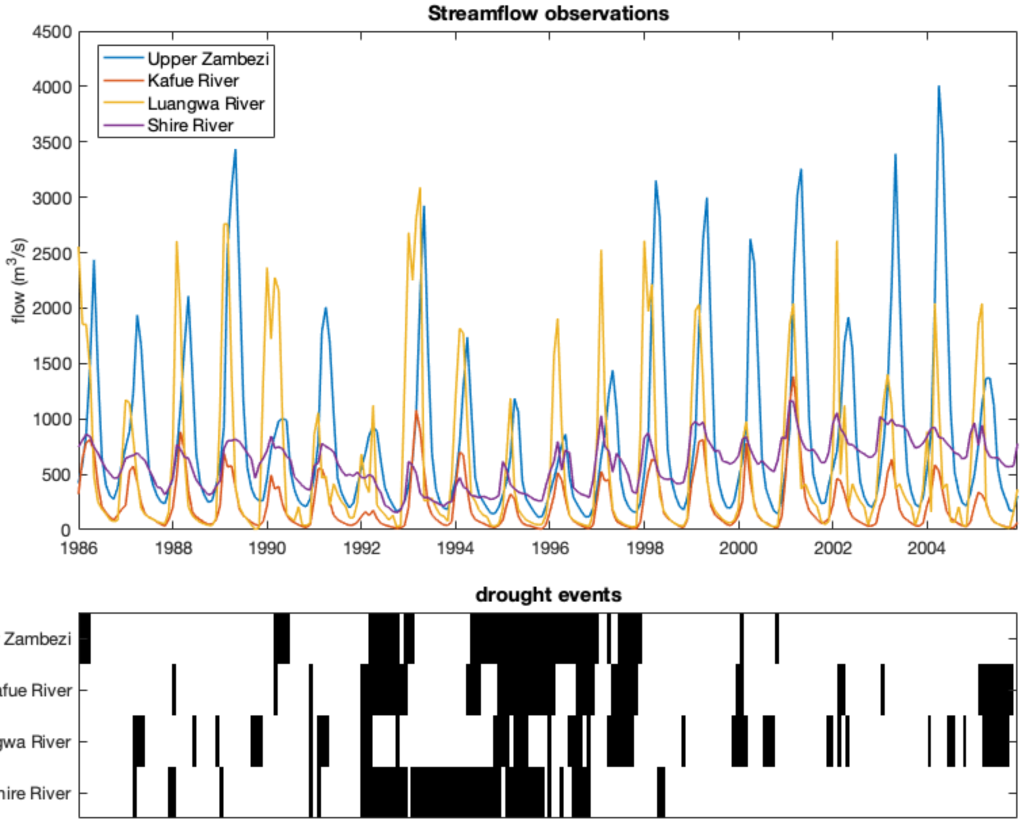

Figure 9 Drought events in the four sub-basins of the Zambezi Watercourse according to the definition adopted by the Zambezi Watercourse Commission. Top: monthly historical observations; Bottom: occurrence of drought events.

5.2.3 Douro River Basin

The prolonged drought index (Figure 10) aims at monitoring hydrometeorological droughts, and it combines the following variables: (i) 6-month cumulative inflows in Barrios de Luna and the inflow to Villameca; (ii) 6-month cumulative discharge in selected gauge stations in natural flow regime; (iii) 9-month cumulative rainfall in selected rain meters. The index is calculated with historical datasets of rainfall and streamflow, using the periods 1980-2012 and 2012-2017 for the computation and validation of the index, respectively. While the rainfall datasets are observations provided by the Spanish National Meteorological Agency, the streamflows are simulated using an impact rainfall-runoff model and, when available, corrected with observations. All data series are normalised and aggregated in a weighted way to produce the prolonged drought index. Rainfall variables are assigned less weight (40%) than streamflow variables (60%). A single threshold value of 0.3 is defined to determine the occurrence of prolonged drought. As seen in Figure 10, the index detects well the dry spells in the system, going under 0.3 for the driest years. The longest, but not the most intense drought, is recorded for the period 1990-1993. The most intense droughts are registered during the last decade, during the periods 2007-2009, 2012 and 2017-2018.

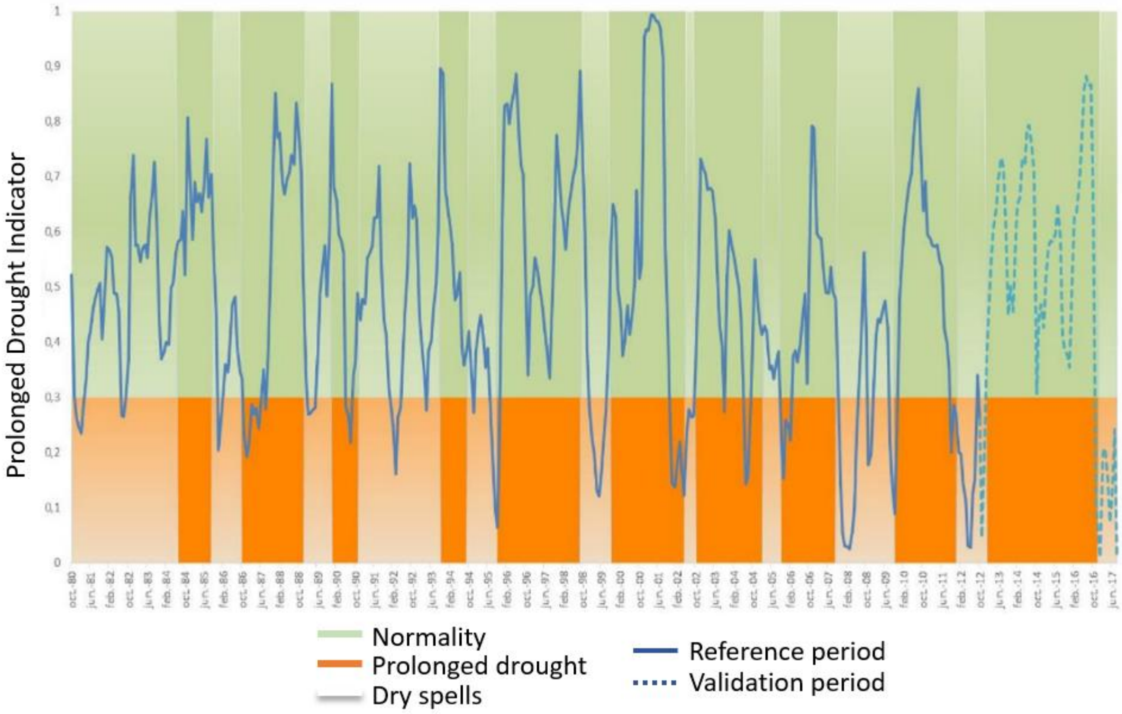

Figure 10 Prolonged drought index evolution in Orbigo system (1980-2017).

The scarcity index (Figure 11) aims at reflecting a temporary problem in meeting water demands, not necessarily caused by hydrometeorological droughts. For this reason, it takes into consideration the levels in Barrios de Luna and Villameca Reservoirs, as well as the monthly existing water demands in the Orbigo system. The levels in the reservoirs are observations for the period 1980-2017. The main water demands are domestic (including industrial), environmental and agricultural. For each reservoir, a supply-demand balance is computed at the monthly scale for the considered period (1980-2017). Then, based on these historical balances, and for every month of the year (e.g., January), three reservoir levels are defined as thresholds to distinguish three different water scarcity states, namely moderate, severe and grave scarcity. These water scarcity states correspond to three different levels of drought risk, namely pre-alert, alert, and emergency. These thresholds are normalised and aggregated in a weighted way to conform to the scarcity index. Barrios de Luna Reservoir is assigned a weight of 0.9 due to its highest regulatory capacity. The scarcity index is very dynamic (see Figure 11), transiting different states within a single year. The years with the most intense water scarcity (emergency level) are 1985-1987, 1992, 1995, 2002, and 2017.

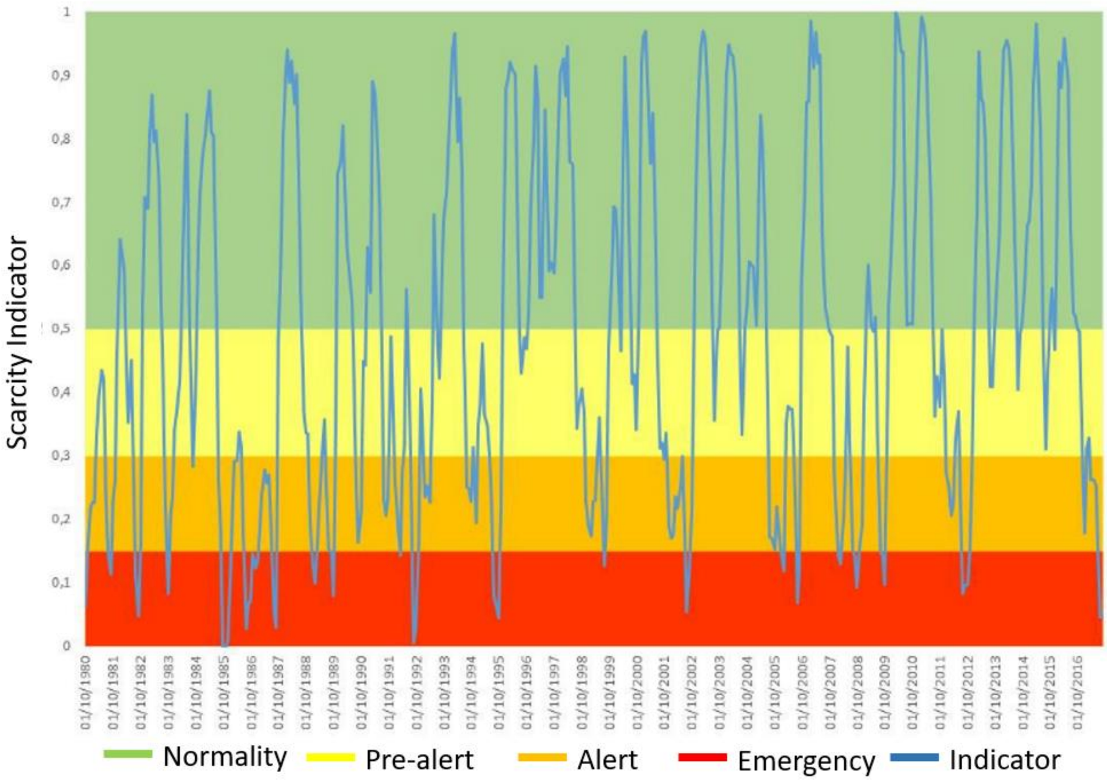

Figure 11 Scarcity index evolution in Orbigo system (1980-2017).

5.2.4 Rijnland

The water board of Rijnland monitors the occurrence of drought events based on a specific user-based definition, which accounts for both precipitation and surface water shortage. More specifically, the water board defines a drought to be onset when the surface water observed at Lobith station (where the Rhine enters the country) is below 1300 m^3/s and when, at the same time, the cumulative precipitation deficit is above 150 mm. The precipitation deficit is defined as the difference between the potential Makkink evapotranspiration and the precipitation, hence an increase in the precipitation deficit is a sign of (meteorological) water scarcity. As meteorological droughts occur most likely in the summer season, the cumulative precipitation deficit is computed every year only from 1st April to 30th September.

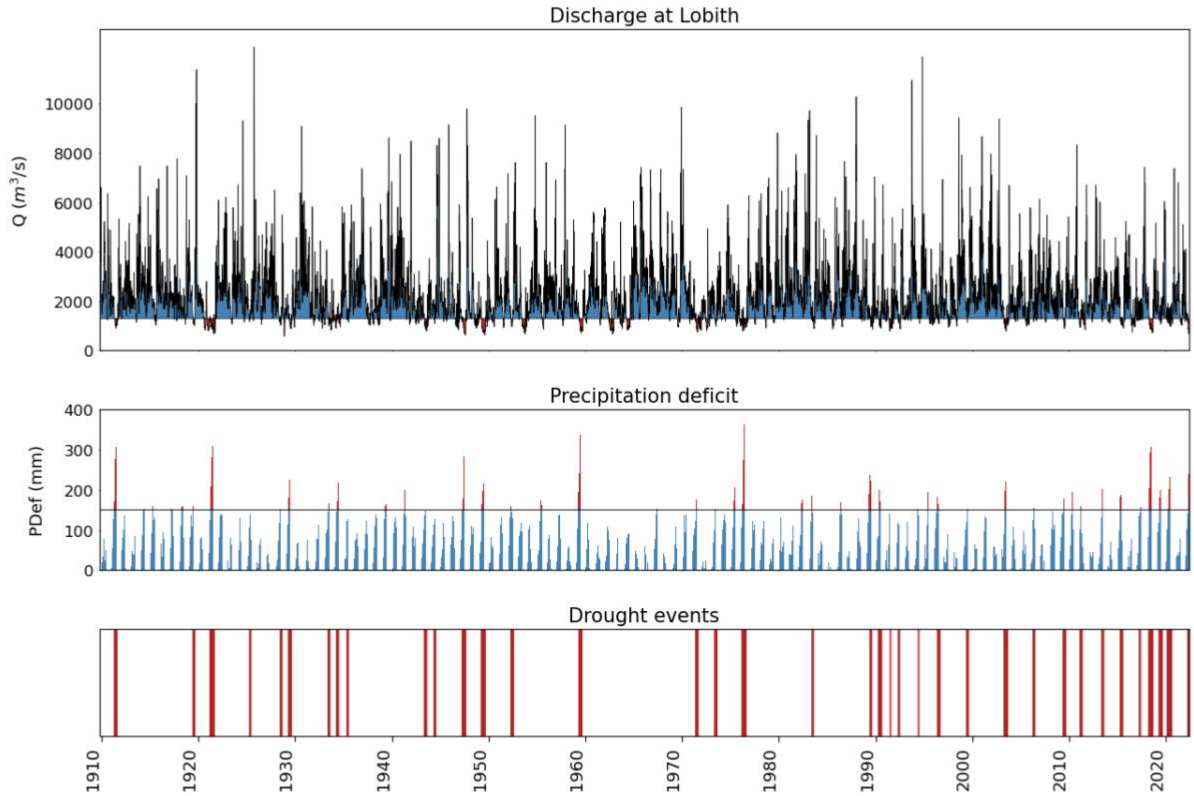

Figure 12 Drought events occurred in Rijnland according to the definition adopted by the water board. Top: daily discharge observations recorded at Lobith station, where the Rhine enters the Netherlands. Areas in red indicate days with flow below the threshold of 1300 m^3/s. Centre: cumulative precipitation deficit computed from ERA5 reanalysis data, each year from the beginning of April to the end of September. Areas in red indicate days with precipitation deficit above the threshold of 150 mm. Bottom: occurrence of drought events in Rijnland. An event starts when the cumulative precipitation deficit is above 150 mm, and at the same time, observed flows in the Rhine are below 1300 m^3/s.

Figure 12 shows the occurrence of drought events from January 1910 to August 2022, based on historical records and according to the definition adopted by the water board. The upper box shows the historical flows recorded at Lobith station, distinguishing the values between those above the minimum threshold (blue) and those below the threshold (red). The graph has been realised using the daily flow time series provided by KNMI for the period 1910-2022, and for the period 2021-2022 by averaging the hourly observations recorded at the same station and provided by the Rijnland water board.
The middle box shows the cumulative precipitation deficit (PDef), as computed each year from the beginning of April to the end of September. In the figure, following the same convention adopted by the water board, when the ongoing deficit reaches negative values, the graph is automatically set to zero and starts showing again data when the ongoing deficit reaches positive values. The analysis is realised by using the daily time series of cumulative precipitation deficit provided by KNMI for the period January 1910- August 2022. This time series has been built by using the daily average precipitation and daily average Makkink evapotranspiration data coming from a set of 13 well-defined stations, and it is representative of the whole country.

The bottom box shows the occurrence of drought events, as defined by the water authority. Vertical red lines indicating that a drought is in place are issued when both the conditions on surface water and precipitation shortage are met. The thicker the lines, the longer the duration of drought. It is worth noting that the box provides information only related to the duration of an event, while it does not give information regarding its severity. By observing this last box, it can be noted that drought events in the last 30 years occurred with a higher frequency with respect to any other similar period in the past, with two of the longest droughts occurring in 2018 and 2020. Other long-lasting events were those of 1921, 1949 and 1976, which are also considered the longest events at the national level. Finally, it should be noted that data from the summer of 2022 were not completely available, hence no conclusion regarding its duration could be made.

Since 2020 KNMI, the meteorological institute of the Netherlands started computing the Standardised Precipitation Index for 1 month (SPI-1) for the whole country for monitoring purposes. However, this indicator has not been adopted yet by Rijnland to define drought events. Figure 13 presents an overview of the SPI-1 index computed from January 1980 to December 2021, by using the reanalysis data of ERA5. The reanalysis data have been spatially averaged within the region of Rijnland. To be consistent with Figure 12, only SPI-1 values from April to September of each year are reported. In Figure 13, values in red mean that a drought is an onset, while values in blue state that the considered month was wetter than normal. As it can be noticed by comparing Figure 12 and Figure 13, using SPI-1 to detect drought results in detecting more events than by using the user-based definition.

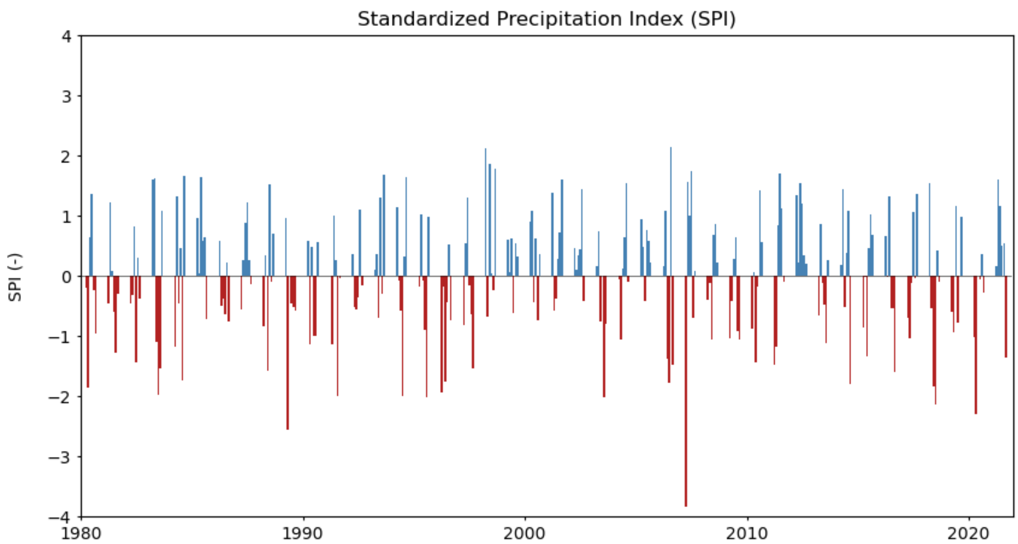

Figure 13 Drought events occurred in Rijnland according to the SPI-1 values computed using ERA5 reanalysis data. Values obtained in the period October-March are omitted to facilitate the comparison with the user-based definition.

5.2.5 Aa en Maas

A complex multi-year drought occurred in the management area of regional water authority Aa en Maas in recent years. The complexity is reflected by drought indices expressing both meteorological and hydrological drought. Figure 14 shows the drought indices for the climatological mean and the years based on local observations. The indices are shown for the growing season in the Netherlands, which is the period between April and October. The precipitation deficit reflects the development of the meteorological drought and is defined as the cumulative sum of the daily precipitation sum minus the daily reference evapotranspiration measured at the Volkel station of the Royal Dutch Meteorological Institute (KNMI). The groundwater levels are visualised relative to the Dutch datum (NAP). The figure shows the groundwater level measures at location ANNA007. The discharge of the Maas river is measured at measurement location Lith. The discharge series are only available up to the year 2019.

All indices show that the years 2018, 2019, 2020 and 2022 were much drier than the climatological mean. Secondly, it is remarkable that the drought develops each year differently. For example, the peak of the 2018 drought is in August, while the peak of the 2022 drought is observed in September. Thirdly, the effect of a drought in a previous year is clearly visible for the groundwater level drought and discharge indices, while not in the meteorological drought (which is reset on April 1st by definition).

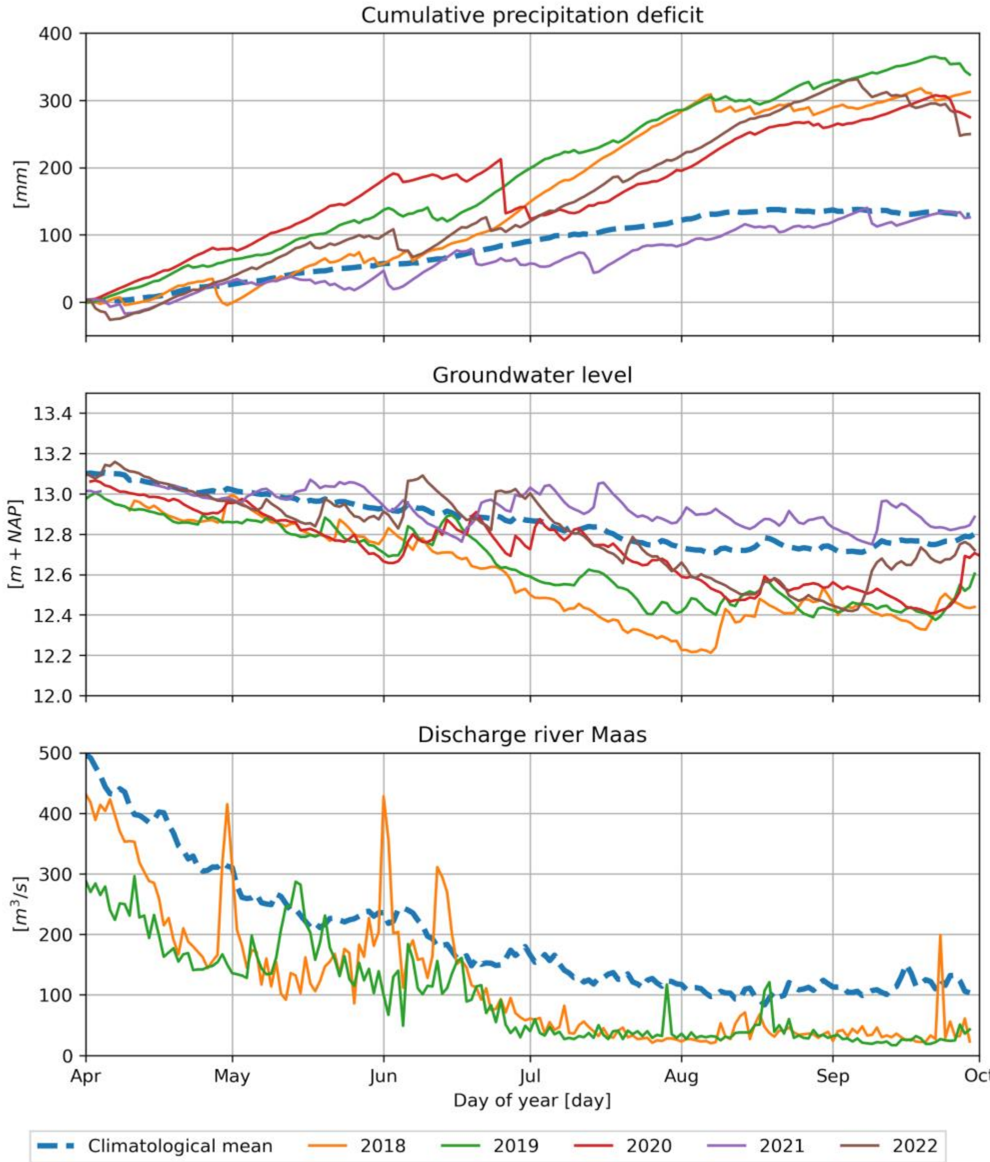

Figure 14 Historical trajectories of drought indices (precipitation deficit, groundwater levels and Maas river discharges) for the management area of regional water authority Aa en Maas in the Netherlands.

5.2.6 Lake Como basin

The authority operating Lake Como (i.e., Consorzio dell'Adda) detects drought events when the monthly net inflows to the lake are below the 10th percentile of the historical observations in that month. The daily net inflows are reconstructed by Consorzio dell'Adda from measures of lake levels and releases from January 1946 to December 2019. The top panel of Figure 15 illustrates the trajectory of monthly inflows obtained by aggregating the daily data provided by Consorzio dell'Adda. The middle panel shows the anomaly of the net inflows with respect to the 10th percentile thresholds, with the negative values (red) identifying drought events. The lower the value, the more

intense the drought event. Lastly, the bottom panel shows the occurrence of drought events that are represented by vertical lines where thick lines mark long events.
The results in Figure 15 show the summers of 1976-2005-2006 as the most intense drought events. Moreover, the bottom panel of the figure illustrates how the period 2003-2007 was characterised by frequent drought events, as discussed in several studies (e.g., Anghileri et al., 2013; Giuliani et al., 2020).

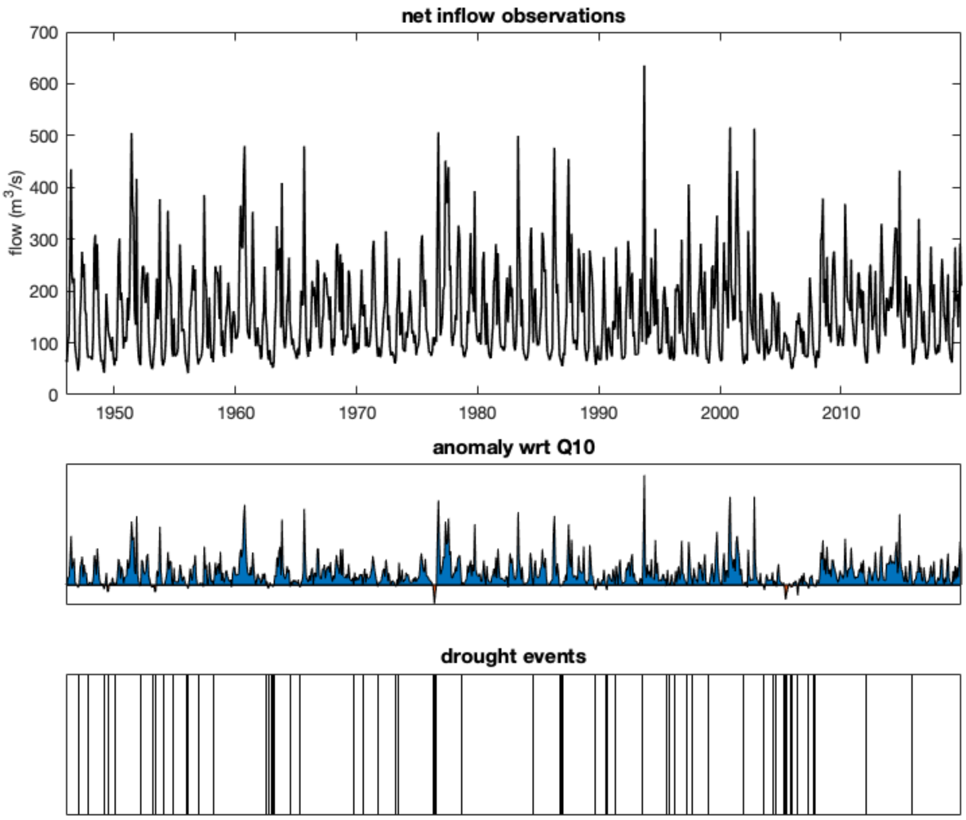

Figure 15 Drought events occurred in Lake Como according to the definition adopted by the lake operator. Top: monthly historical observations; Middle: anomaly of monthly inflow with respect to the 10th percentile (Q10) of the historical values in the same month; Bottom: occurrence of drought events.

5.3 Datasets for drought detection

The computation of drought indices in the CLINT Climate Change Hotspots will be mostly based on local observations. Besides, a number of global/continental datasets will be used in Task T3.3 for the analysis of extreme droughts over the European domain.

5.3.1 HydroGFD2.0

In Task T3.3, we will use the Hydrological Global Forcing Data (HydroGFD2.0; Berg et al., 2018) as a dataset of precipitation and temperature for the detection of extreme droughts over the European domain. HydroGFD is a merged data set of historical precipitation and temperature from meteorological reanalysis and global observations. The reanalysis system from ECMWF uses atmospheric and surface observations to reproduce the observed weather and climate as closely as possible on a global scale. However, the reanalysis product has a bias that prevents its direct use in hydrological models, and consequently, HydroGFD is carrying out bias adjustments to remedy such issues.

With HydroGFD2.0, the baseline climatology is first calculated for the period 1981-2009, combining satellite and station-based observations. GPCCv7 (Schneider et al., 2014), CPC-Unified (Chen et al., 2008) and CRUts4.0 data set from the Climate Research Unit (CRU; Harris and Jones, 2017) are used for adjusting precipitation amount and number of wet days, whilst CRUts4.0 and CPC-Temp (CPCtemp, 2017) products are used for temperature adjustments. Absolute monthly mean data are then calculated by adding anomalies from different data sets to the climatology. Common for all variables are the resolution of 0.5 degrees (about 50 km) on a regular global grid and the time period 1961 until present using reanalysis systems ERA40 (1961-1978) and ERA-Interim (1979 until present). Bias adjustments are only performed over land areas included in the observational data, and oceans default to the original reanalysis data.

Bias adjustment is performed separately for every single month with monthly mean precipitation, number of wet days, and temperature. This leads to a data set of daily values of precipitation and daily mean, minimum and maximum temperature.

5.3.2 Historical Simulations of E-HYPE

HYPE (HYdrological Predictions for the Environment) is a continuous semi-distributed process-based model, which simulates components of the water cycle (i.e., snow accumulation and melting, evapotranspiration, soil moisture, streamflow generation, groundwater recharge, and routing through rivers and lakes) at a daily time step (Lindström et al., 2010). Meteorological variables of daily mean precipitation and temperature derived from the HydroGFD product v2.0 were used to drive the hydrological model for the period 1993–2018.

E-HYPE reproduces streamflow and water balance over the Pan-European region with ~35,400 catchments. Its parameters were calibrated based on a set of 115 catchments representing the diversity of land use and soil characteristics, as well as human impacts. The model was validated in about 550 catchments for which streamflow observations are available. The performance of E-HYPE in validation in terms of streamflow reaches a median Nash-Sutcliffe Efficiency of 0.53 over Europe. Details about the model performance can be found in Hundecha et al. (2016).

The streamflow and soil moisture outputs from historical simulation of the E-HYPE will be used for the computation of SRI and SSI indices over the European domain during the time period 1993-2018. Importantly, this dataset is consistent with the HydroGFD2.0 climatic forcing used for computing SPI and SPEI indices.

5.3.3 E-HYPE seasonal hydrometeorological service

The ability of the E-HYPE seasonal hydrometeorological service in detecting and predicting extreme droughts will be used as a benchmark to quantify the potential added value of the AI-enhanced methods developed in Task T3.3 in collaboration with Tasks T2.1 and T2.4. Notably, the ECMWF SEAS5 and CMCC seasonal precipitation and mean temperature forecasts are bias adjusted using the Distribution-Based Scaling (parametric quantile mapping) method (Yang et al., 2010) prior to

being introduced as forcing input in the E-HYPE hydrological model, using HydroGFD2.0 data (see Section 3.1) as a reference for the bias adjustment.
Forecasts are provided at sub-basin resolution (polygon with an average size of 215 km2) and grid resolution (5 km x 5 km grid) over the time period 1993-2015, with the model initialised at the beginning of each month. The hydrological forecasts forced by ECMWF SEAS5 (~ 7-month lead time) and CMCC (~ 6 -month lead time) consist of 25 and 40 ensemble members, respectively (see Table 13).

Table 13 List of seasonal forecast datasets used in Task 3.3.

Name	Source	Handled by	Processed by	Stored by	Used by
ECMWF SEAS5	C3S-CDS	SMHI	SMHI	SMHI	SMHI, POLIMI
CMCC SPS3.5	C3S-CDS	CMCC, SMHI	SMHI	SMHI	SMHI, POLIMI
E-HYPE simulations	SMHI	SMHI	SMHI	SMHI	SMHI, POLIMI

5.4 Candidate drivers for extreme drought detection

Based on the literature, the following local and large-scale phenomena are considered as potential drivers for extreme drought detection (and potentially prediction):

- **Hydrologic conditions**: They represent local conditions' influence on local water availability. Depending on the characteristics of the region under investigation, it could be useful to consider snow-related variables (e.g., Staudinger et al., 2014), such as snow cover, snow height, snow water equivalent, as well as high temperatures that increase the fraction of precipitation falling as rain instead of snow and advance the timing of spring snowmelt (Douvielle et al., 2021); water volume stored in lakes and artificial reservoirs (e.g., Haro et al., 2014); groundwater level (e.g., Bloomfield and Marchant, 2013); atmospheric evaporative demand that affects evapotranspiration and soil moisture (Vicente-Serrano et al., 2020).
- **Atmospheric conditions**: The state of the Northern Hemisphere polar vortex can influence the position of the jet streams, the position of the storm tracks, and the atmospheric circulation at the surface. Persistent anomalies of the polar vortex can lead to anomalous precipitation patterns over several months, in particular during wintertime (Ayarzagüena et al., 2018; Domeisen and Butler, 2020). Blocking conditions can represent key atmospheric factors in the development of large-scale heat waves and droughts, which trigger soil-moisture temperature feedbacks (Toreti et al., 2019a)
- **Teleconnection and climatic patterns**: They generate interactions and/or feedbacks with other components of the climate system, potentially amplifying the severity of the event. In particular, the literature suggests extreme droughts could be linked with:

- El Nino Southern Oscillation (e.g., Vicente-Serrano et al., 2011)
- North Atlantic Oscillation (e.g., Tsanis and Tapoglou, 2019)
- Sea Surface Temperature (e.g., Forootan et al., 2020; Garrido-Perez et al., 2022)

6 COMPOUND EVENTS AND CONCURRENT EXTREMES

6.1 Overview

Quantifying the probability of future extreme events is important for adaptation planning, for instance, in the agricultural sector, for fisheries, river transport as well as for energy supply (Zscheischler and Fischer 2020). Given that future predictions indicate a rise in the frequency of many types of extreme events (IPCC 2022), the latter becomes increasingly important. While human and natural systems have a certain resilience against single extreme events, they might be unable to sustain multiple extreme events as their impacts tend to amplify in a non-linear relationship (Zscheischler et al. 2018; Zscheichler et al. 2020). Furthermore, it is crucial to accurately examine the association or connections between these types of events because the risk and return periods of extreme events might be considerably underestimated when one assumes independence of these occurrences or simply investigates a single extreme event (Wahl et al. 2015; Zscheischler and Seneviratne 2017).

Compound events are frequently referred to in the literature as a combination of extreme events and the concomitant (possibly non-extreme) phenomena of these types of events that contribute to the socio-economic damage of this event. To be more precise, Zscheischler et al. 2018 define a compound event as:

“The combination of multiple drivers and/or hazards that contributes to societal or environmental risk.”

Typologies have been developed to further categorize the dependence structure of compound events (Zscheischler et al. 2020; Bevacqua et al. 2021). The definition above highlights the multivariate nature of these types of events, but it should be recognized that the involved events do not necessarily have to be extreme events.

Toreti et al. 2019b described a subset of compound events named concurrent extreme events, where the emphasis is on the dependencies of extreme events. They define a concurrent extreme event as

“Extremes of different types occurring within a specific temporal lag, either in different locations or at the same one, as well as by extremes of the same type occurring in two different locations within a specific time period.”

To ensure a coherent risk assessment of high-risk events such as compound events, multiple drivers should be considered that play a synergistic and reinforcing role. The increasing frequency, severity and extent of these impacts have also increased scientific interest in the events that lead to these impacts, compound events and concurrent extremes (for a review, see, for instance, Leonard et al. 2014; Hao et al. 2018; Zscheischler et al. 2018; Raymond et al. 2020; Zscheischler et al. 2020; Zhang et al. 2021). To our knowledge, however, the use of artificial intelligence (AI) and ML has been yet relatively underrepresented in the analysis of compound events, and CLINT aims at filling this gap by developing AI- and ML-based techniques together with hybrid approaches (a combination of the former with well-known statistical methods) for the detection, causality, and attribution study of compound events and concurrent extremes.

This chapter introduces the detection methods for the analysis of compound events and concurrent extremes, as well as the datasets and drivers that will be utilized for that purpose in Task 3.4.

6.2 Detection of compound events and concurrent extremes

6.2.1 Compound events

Within Task 3.4.1, the following types of compound events related to important impacts in the water, energy and food sectors will be analyzed:

a) Warm and relatively wet late winters followed by dry and warm springs with severe impacts on agriculture.

b) Dry winters followed by hot summers, which accumulate pressure on the agricultural and the energy sectors with direct impacts on the hydropower capacities during the increased demand period.

c) Wet and warm springs with impacts on water management, increased flood risk due to precipitation excess and early melting season.

Compound events, without necessarily being extreme, have significant socioeconomic impacts, and hence their study should combine their impacts and the climatological phenomenon (Zscheischler et al. 2018). The analysis of compound events under the CLINT framework concentrates on impact indicators on the three sectors, water, energy and food, considered within work package 6, with the goal of identifying the relevant drivers of those impacts using AI/ML methodologies. The assumption is that since compound events are, by definition, associated with the most severe impacts, the AI method will discover their pattern through the impacts used as the basis for defining the compound events above.

The dependencies among these drivers will then be examined using traditional multivariate statistics, such as Markov and Bayesian networks (e.g., Hastie et al. 2017; Sperotto et al. 2017), vine-copulas (e.g., Hao et al. 2018; Czado and Nagler 2022) or “synergies” of the two techniques (e.g., Elidan 2013; Couasnon et al. 2018). In order to further emphasize the significance of evaluating the connectivity among the drivers, return periods will be constructed under the assumptions of independence and dependence, as it is frequently found that return periods can significantly decrease when an extreme multivariate framework (with dependent drivers) is employed (e.g., Zscheischler and Seneviratne 2017).

6.2.2 Concurrent extremes

The analysis within CLINT will focus on the connectivity of large-scale droughts and heatwave events at the global scale. The large-scale extreme events are defined following Toreti et al. (2019b): Firstly, for given regions of interest, heatwaves and droughts will be identified on the grid scale using statistical extreme event detection approaches (e.g., through threshold exceedances of indices). Subsequently, the time points are collected at which a certain number of grid points (e.g., 20 %) within a considered region fulfil the given criterion that classifies the time points as occurrences of large-scale extreme events. Hence, for heatwave and drought events, a set of time points is obtained for specific regions, which are then modelled as a marked point process (see, e.g., Daley 2003; Daley and Vere-Jones 2008). The interdependencies of these events can then be evaluated using the marked inhomogeneous J-Function (Cronie and van Lieshout 2016), which can determine whether the obtained time points exhibit clustering, inhibition, or independence. The latter also allows for a non-constant occurrence of these events over the considered time interval and is, therefore, able to take the non-stationarity of the climate into account. By analysing the above time occurrences depending on the phase of a teleconnection state under consideration (e.g., El Nino and La Nina for ENSO), links to teleconnections (such as ENSO, NAO) can also be employed As previously stated, the detection of the drought and heatwave events at the grid scale will be accomplished following Tasks 3.2 and 3.3 by using heatwave and drought indices such as the HMD and the HWS, the SPI and the SPEI (see Tables 7 and 11) or AI-enhanced versions of the later developed within Tasks 3.2 and 3.3. By applying a cluster analysis like k-means (e.g., Hastie et al. 2017) or extreme values theory-based approaches (Bernard et al. 2013; Bador et al. 2015) to the indices, it will be possible to pinpoint the areas with similar drought and heatwave patterns, which will then serve as the regions of interest.

Table 14 List of the indices for heatwaves and droughts detection at European & global scale for concurrent extremes in Task 3.4.

Acronym	Name	Essential climate variables	Description	References
SPI	Standardized Precipitation Index	Precipitation	SPI represents the number of standard deviations the cumulative precipitation deviates from the average of a standardized normal distribution.	McKee et al. (1993); Hayes et al. (1999)
SPEI	Standardized Precipitation and Evapotranspiration Index	Precipitation and Potential Evapotranspiration	SPEI represents the deviations from the average of a standardized distribution but replaces the precipitation data with the difference between precipitation and potential evapotranspiration. SPEI is also appropriate for arid climates, where evapotranspiration has a key role in depleting soil moisture.	Beguería et al. (2010); Vicente-Serrano et al. (2010); Beguería et al. 2014
HMD	Heat Magnitude Day	Tmax (daily maximum 2-meters temperature)	Accumulates heat wave magnitude (as in Russo et al. 2015) for the 3-month period before the harvesting season, representing heat stress within this period.	Zampieri et al. (2017); Toreti et al. (2019b)
HWS	Heat Wave Severity	Tmax or Tmin (daily maximum/minimum 2-meters temperature)	Accumulated temperature exceedance (above the local 90th percentile) for all heat wave days (temperature exceeding the 90th percentile) over a user-defined interval (monthly, seasonal, etc.	Perkins-Kirkpatrick and Lewis (2020)

***Acronym** = Abbreviation used for the index, **Name** = full name of the index, **Essential climate variables** = variables required for the computation of the index, **Description** = short definition of the index, **References** = Publications where the index is used and/or defined.*

6.3 Datasets for compound events and concurrent extremes

The datasets used for the study of compound events and concurrent extremes in CLINT comprise reanalysis data with high spatial and temporal resolution and the longest possible temporal coverage, climate model outputs, surrogate data required for the concurrent extremes, as well as impact data for the water, energy and food security nexus sectors.

6.3.1 Climate data for compound events and concurrent extremes

6.3.1.1 ERA5

See 2.3.1.

6.3.1.2 ERA-20C

See 4.3.2.

6.3.1.3 20CRv3

See 4.3.3.

6.3.1.4 CMIP6 and PMIP4

The training of the AI algorithms can be further augmented by using global bias-corrected for the concurrent extremes and European bias-corrected and downscaled for the compound events and climate model simulations from CMIP6. CMIP's objective is to better understand past, present and future climate change arising from natural (unforced) variability or in response to changes in radiative forcing (Eyring et al. 2016). Within Task 3.4, the analysis is going to focus on historical simulations for the models listed in Table 15.

Table 15 List of CMIP6 model simulations used in Task 3.4.

Name	Source	Handled by	Processed by	Stored by	ETD	Used by
CESM2	ESGF	JLU	JLU	JLU	August 31, 2022	JLU
CNRM-CM6-1-HR	ESGF	JLU	JLU	JLU	August 31, 2022	JLU
EC-Earth3	ESGF	JLU	JLU	JLU	August 31, 2022	JLU
GFDL-ESM4	ESGF	JLU	JLU	JLU	August 31, 2022	JLU
HadGEM3-GC31-MM	ESGF	JLU	JLU	JLU	August 31, 2022	JLU
MPI-ESM1-2-HR	ESGF	JLU	JLU	JLU	August 31, 2022	JLU

Name	Source	Handled by	Processed by	Stored by	ETD	Used by
NorESM2-MM	ESGF	JLU	JLU	JLU	August 31, 2022	JLU

***Name** = short name of the dataset, **Source** = original producer, **Handled by** = partner doing the download/extraction of the dataset over the region of interest, **Processed by** = partner applying any "model output statistics" if any (downscaling, calibration etc.), **Stored by** = partner distributing the data for the consortium partners (e.g., centralised CLINT repository at DKRZ), if need be, **ETD** = estimated date of availability (from handling/storing partner), **Used by** = partner using the data (case study).*

Task 3.4 will also use longer model simulations from CMIP6 and the Paleoclimate Modelling Intercomparison Project phase 4 (PMIP4). The model simulations (Table 16) are externally forced following the protocol by Jungclaus et al. (2017). The forcings between 500 BC and 1 AD are according to the Bader et al. (2020) simulation (i.e. the Holocene simulation).

Table 16 List of PMIP4/CMIP6 simulations used in Task 3.4.

Name	Source	Handled by	Processed by	Stored by	ETD	Used by
MPI-ESM-LR-P	Hereon	Hereon	JLU	JLU	August 31, 2022	JLU
MPI-ESM-LR Mythos (500 BCE - 1850 CE)	Hereon/JLU	JLU	JLU	JLU	August 31, 2022	JLU
MPI-ESM-LR 2k	ESGF	MPI-M	JLU	JLU	August 31, 2022	JLU

***Name** = short name of the dataset, **Source** = original producer, **Handled by** = partner doing the download/extraction of the dataset over the region of interest, **Processed by** = partner applying any "model output statistics" if any (downscaling, calibration etc.), **Stored by** = partner distributing the data for the consortium partners (e.g., centralised CLINT repository at DKRZ), if need be, **ETD** = estimated date of availability (from handling/storing partner), **Used by** = partner using the data (case study).*

6.3.2 Concurrent extremes data

6.3.2.1 Surrogate data

The inhomogeneous J-Function will be utilized to examine the connectivities of large-scale drought and heatwave events for the analysis of concurrent extremes. The J-Function, as previously stated, can categorize these connectivities into three types of dependence structures: clustering, inhibition, and independence (see, e.g., Baddeley et al. 2016). However, the decision as to which class a specific J-function belongs to is still determined by the user and is thus exposed to subjectivity. The main objective for Task 3.4.2 within CLINT is thus to develop an AI-based automated interpretation tool for the J-Function that can classify a given J-Function to a dependency structure from above and estimate the change point in dependence. For this, Monte Carlo simulations will be used to simulate data sets which mimic these three types of dependence structures. Then for each simulated data set, the dependence structure can be labelled such that the problem becomes a classification problem and an AI model can be trained.

Point process models for which the J-Function has the desired features are going to be used, and the simulation setup of van Lieshout (2011) and Cronie and van Lieshout (2015) is going to be adopted. They show that the J-Function has the desired properties by using a log-gaussian cox process model for clustering, an inhomogeneous point process for independence, and a thinned hardcore process for inhibition (for a description of the processes, see, for instance, González et al. 2016 and the references within). Furthermore, non-stationary intensity functions (see, for instance, Diggle 2014) will be employed, as they are more likely to occur in climatic data sets (Toreti et al. 2019a; Toreti et al. 2019b). For each simulated data set, the J-Functions are then estimated following van Lieshout 2011, Cronie and van Lieshout 2016 and Moradi et al. 2019 together with a perturbation method developed in Toreti et al. 2019b.

6.3.3 Compound events data

As previously stated, data sets identifying the impact of compound events on the food, energy, and water sectors will be used for Task 3.4.1 and will be adopted from MS15. The data sets will be described in the following sections.

6.3.3.1 Food - ECroPS, FAOSTAT, Eurostat

ECroPs

Crop yield simulations using the ECroPS dynamical process-based crop model (Toreti et al. 2019c) will be utilized to assess the impact on the food sector. The ECroPS modelling framework was created to address the high computational demand of high-resolution regional climate model simulations and is tailored to run in MPI environments. The ECroPS crop simulation model is based on the WOFOST crop simulation model (Wit et al. 2019), but with new important parameterization methods, which are the response to elevated CO2 concentrations and the impact of heat stress on flowering.
The core of ECroPS consists of a mechanistic crop growth model that explains crop growth in terms of underlying processes like photosynthesis and respiration, as well as how these processes are influenced by environmental variables. Furthermore, the impact of highly relevant climate extremes is simulated, including heat stress and droughts. Modules in ECroPS include phenological development, light interception, gross CO_2 assimilation, growth and maintenance respiration, dry matter partitioning, source and sink limited leaf area development, soil water balance and soil nutrition balance. The crop model is parameterized to allow for regional heterogeneity in the crop model parameters across Europe, thus taking into account differing spatial variety distributions for the major crops (Ceglar et al. 2019). The latter is based on a pan-European spatial calibration of several crop model parameters related to variety prevalence in various European growing regions. Finally, ECroPS distinguishes three levels of crop production: potential production (determined by crop variety, radiation and temperature), water-restricted production (water availability limits potential production) and nutrient-limited production (in which nutrient availability limits water-limited production).

FAOSTAT

The United Nations established the Food and Agriculture Organization (FAO; https://www.fao.org/) as a specialized organization with the aim of attaining global food security and ensuring access to sufficient and quality food. FAO is active in 130 countries around the world and has 195 members. FAOSTAT provides free access to food and agricultural data for 245 countries - including the European domain - from 1961 to the present. The data is mainly obtained through questionnaires submitted to members on a regular basis. The data includes statistics on agricultural production, food security and nutrition, food value chain, as well as climate change, among other domains.

Eurostat

Eurostat (https://ec.europa.eu/eurostat) is the statistical office of the European Union, with the aim of providing high-quality statistics and data on Europe. The statistics are produced in cooperation with the national statistical institutes and other national authorities in the EU Member States, known as the European Statistical System (ESS). The statistical authorities of the European Economic Area (EEcA) and Switzerland are also part of the ESS. In recent decades, new indicators and statistics that reflect changes in EU policies have been introduced, enhancing the initial aim of monitoring the EU's Common Agricultural Policy (CAP) main objectives (e.g., Hill 2012). Agricultural statistics in Eurostat provide information on the topics of farms' structure, the economic accounts for agriculture, prices and prices' indices, agricultural production and organic farming, as well as agriculture and the environment.

CLINT will use the above-described data sources to study the impacts of compound events on the food sector, and adequate impact indicators will be adapted from MS15. The analysis will further follow MS4 and support WP6 objectives and will focus on climate impacts of the three main crops grown in Europe: winter soft wheat, grain maize and winter barley. Additionally, AGRI4CAS's data portal (https://agri4cast.jrc.ec.europa.eu/DataPortal/Index.aspx) will be used to acquire the agrometeorological variety zones for the main crops in Europe (Ceglar et al. 2019).

6.3.3.2 Water – E-Hype

The high-resolution pan-European water model E-HYPE (Donnelly et al. 2016; Hundecha et al. 2016) calculates hydrological variables on a daily time-step and calculates water balance, hydrological variable dynamics, and daily discharge for continental Europe. It is maintained and operated by SMHI, a governmental organization under the Ministry of Environment. It can be used for a variety of purposes, including hydrological forecasting, environmental flow management, infrastructure development planning, and assessing the impact of climate change (Wallman et al. 2011). Input data includes Global Monitoring for Environment and Security (GMES) satellite products, global data sets (e.g., topographic, land use, soil type, precipitation and temperature data), meteorological data, climate projections, policy scenarios, and local data. Many hydrological variables, such as water balance, flow rates and depths (when rating curves or hydrographic data are available) in all major streams and rivers in Europe, soil moisture level, lake/reservoir depths and levels, snow depths, snow water equivalent and regional snow coverage are produced at high resolution by the model. Furthermore, statistics for the predicted and observed data can be provided as regional statistics and individual sites.

6.3.3.3 Energy - PRIMES

The Price-induced market equilibrium system PRIMES model, developed by E3Modelling, a spin-off of the E3MLab at the National Technical University of Athens (NTUA), can simulate medium- and long-term (up to 2070) projections in five-year steps (MIDAS @JRC website 2021). It is applicable to all European Union member states, European Free Trade Association (EFTA) nations (except Lichtenstein), and candidate countries.

The essential feature of the model is its combination of behavioural modelling (based on a microeconomic foundation) and engineering aspects, which covers all energy sectors and markets and can handle numerous policy objectives (e.g., Greenhouse Gas, GHG emission reductions, energy efficiency, renewable energy targets) (PRIMES 2018). Furthermore, it provides a pan-European simulation of internal markets for electricity and gas. It has been used to conduct impact assessments for the European Commission, including the EU Long-Term Strategy, as well as to develop the "Reference outlook for EU energy, transport, and GHG emission trends to 2050." The input of the model consists of Eurostat and European Environment Agency (EEA) data (e.g., energy balance sheets, energy processes, macroeconomic and sectoral activity data), technological databases, power plant inventory, Renewable energy sources (RES) capacities, potential and availability, network infrastructure and other databases; see MIDAS @ JRC website 2021 for further information. The output of the PRIMES model contains detailed energy balances of the energy system, as well as accompanying CO2 emissions for each country or the EU as a whole. Together with the Greenhouse Gas - Air Pollution Interaction and Synergies (GAINS) and Global Biosphere Management Model (GLOBIOM) models, it is also able to provide comprehensive GHG balances for each country and the EU as a whole (MIDAS @JRC website 2021).

Table 17 List of surrogate and sectoral data used in Task 3.4.

Name	Source	Handled by	Processed by	Stored by	ETD	Used by
Surrogate Data	JLU	JLU	N/A	JLU	August 31, 2022	JLU, UAH
E-HYPE	SMHI	SMHI	N/A	SMHI	August 31, 2022	JLU, POLIMI
ECroPS	JRC	JRC	N/A	JLU	August 31, 2022	JLU, POLIMI
PRIMES	E3M	E3M	N/A	E3M	August 31, 2022	JLU, POLIMI

Name *= short name of the dataset,* ***Source*** *= original producer,* ***Handled by*** *= partner doing the download/extraction of the dataset over the region of interest,* ***Processed by*** *= partner applying any "model output statistics" if any (downscaling, calibration etc.),* ***Stored by*** *= partner distributing the data for the consortium partners (e.g., centralised CLINT repository at DKRZ), if need be,* ***ETD*** *= estimated date of availability (from handling/storing partner),* ***Used by*** *= partner using the data (case study).*

6.4 Candidate drivers for compound events and concurrent extremes

Compound weather and climate events describe combinations of multiple climate drivers and/or hazards that contribute to societal or environmental risk. These events arise from complex interactions between various physical processes across multiple spatial and temporal scales. This work aims at revealing the drivers of the hazards and the physical processes by which weather- and climate-related hazards combine to improve their detection, predictability, causality and attribution through the assessment of the impacts in the sectors of water, energy and food. The climate phenomena are characterised by deviations from mean conditions without being extreme in the statistical sense.

Warm and dry conditions are often linked through land-atmospheric feedbacks (Miralles et al. 2019). In a recent review, Zhang et al. (2021) identified persistent blocking highs, subtropical highs, atmospheric stagnation events, and patterns of planetary heat waves as drivers of warm and dry conditions. For example, stagnation events cause a lack of convection and movement of air masses (Horton et al. 2014; Zou et al. 2020) and blocking highs increase temperature and evapotranspiration while suppressing precipitation (Dong et al. 2018; Schumacher et al. 2019). These conditions can be further intensified by preconditions such as low soil moisture through soil moisture-atmosphere interaction (Berg et al. 2015), dry soil and plants, which reduce evapotranspiration (Seneviratne et al. 2006), and downwind drought conditions, whereby advection of air masses can cause abrupt increases in air temperature and soil desiccation (Schumacher et al. 2019). Other studies have found that concurrent heatwaves in the Northern Hemisphere can be linked to amplified Rossby wave patterns (Kornhuber et al. 2020), whereas warm and dry events in Europe can be related to a Rossby wave train propagating from the United States to Russia (Ionita et al. 2021). Warm and dry events can also be related to **slow varying factors**, as teleconnection patterns like ENSO, which was for instance shown in South Africa (Hao et al. 2019), South America (Cai et al. 2020) and the USA (Hoerling et al. 2013). ENSO and the Indian Ocean Dipole (IOD) have also been shown to have an effect on these types of events in Australia (Reddy et al. 2022). Over western North America during the boreal summer, these types of events have been shown to be positively influenced by the PDO, whereas associations of these types of events with the NAO were relatively weak (Mukherjee et al. 2020). Additionally, it has been demonstrated that strongly negative PDO phases and positive Atlantic Multidecadal Oscillation (AMO) phases favour warm and dry events in the southwest of the United States (Chylek et al. 2014). Concerning future projections, it is found that, with global warming, the frequency of warm and dry events is expected to rise (Zscheischler and Seneviratne 2017; Alizadeh et al. 2020; Vogel et al. 2020; Meng et al. 2022). For instance, it was shown that record-breaking summers like the one that occurred in Central Europe in 2018 can become the norm until the middle of the twenty-first century (Toreti et al. 2019a) and could not have occurred without human influence (Vogel et al. 2019).

Warm and wet events are often modulated when temperature rises over open water bodies, increasing surface humidity (Zhang et al. 2021). On land, however, this effect may be limited by the lack of soil moisture (Fischer and Knutti 2013). A recent review of Zhang et al. 2021 identifies the following drivers of warm and humid events: Irrigation, external forcing such as greenhouse gases and volcanic eruptions and urbanization. Other studies have linked warm, humid conditions to persisting blocking patterns, reduced cloud cover, and the advection of warm air, which can originate in tropical areas (Katsafados et al. 2014; Freychet et al. 2017; Russo et al. 2017). Although there appears to be fewer studies on these types of occurrences than on warm and dry ones, the frequency of warm and humid events is expected to rise (Russo et al. 2017; Wang et al. 2021; Meng et al. 2022) highlighting the need of studying these types of events.

REFERENCES

Alizadeh, M. R., Adamowski, J., Nikoo, M. R., AghaKouchak, A., Dennison, P., & Sadegh, M. (2020). A century of observations reveals increasing likelihood of continental-scale compound dry-hot extremes. Science advances, 6(39), eaaz4571, doi: 10.1126/sciadv.aaz4571

Anghileri, D., Castelletti, A., Pianosi, F., Soncini-Sessa, R., & Weber, E. (2013). Optimizing watershed management by coordinated operation of storing facilities. Journal of Water Resources Planning and Management, 139(5), 492-500, doi: 10.1061/(ASCE)WR.1943-5452.0000313

Ardilouze, C., Batté, L., Déqué, M., van Meijgaard, E., & van den Hurk, B. (2019). Investigating the impact of soil moisture on European summer climate in ensemble numerical experiments. Climate Dynamics, 52(7), 4011-4026, doi:10.1007/s00382-018-4358-1

Asch, A., J. Brady, E., Gallardo, H., Hood, J., Chu, B., & Farazmand, M. (2022). Model-assisted deep learning of rare extreme events from partial observations. Chaos: An Interdisciplinary Journal of Nonlinear Science, 32(4), 043112, doi: 10.1063/5.0077646

Ayarzagüena, B., Barriopedro, D., Garrido-Perez, J. M., Abalos, M., de la Cámara, A., Calvo, N., Ordóñez, C. (2018). Stratospheric connection to the abrupt end of the 2016/2017 Iberian drought. Geophysical Research Letters, 45(22), 12-639, doi: 10.1029/2018GL079802

Baker, A. J., Hodges, K. I., Schiemann, R. K. H., & Vidale, P. L. (2021). Historical variability and lifecycles of North Atlantic midlatitude cyclones originating in the tropics. Journal of Geophysical Research: Atmospheres, 126, e2020JD033924, doi: 10.1029/2020JD033924

Baddeley, A., Rubak, E. and Turner, R. (2016), *Spatial point patterns: Methodology and applications with R, Chapman & Hall / CRC Interdisciplinary Statistics*, CRC Press Taylor & Francis Group, Boka Raton, London, New York.

Bader, J., Jungclaus, J., Krivova, N., Lorenz, S., Maycock, A., Raddatz, T., Schmidt, H., Toohey, M., Wu, C.-J. and Claussen, M. (2020). Global temperature modes shed light on the Holocene temperature conundrum. *Nature communications*, *11*(1), 4726, doi:10.1038/s41467-020-18478-6

Bador, M., Naveau, P., Gilleland, E., Castellà, M., & Arivelo, T. (2015). Spatial clustering of summer temperature maxima from the CNRM-CM5 climate model ensembles & E-OBS over Europe. *Weather and climate extremes*, *9*, 17-24, doi: 10.1016/j.wace.2015.05.003

Beguería, S., Vicente-Serrano, S. M., & Angulo-Martínez, M. (2010). A multiscalar global drought dataset: the SPEIbase: a new gridded product for the analysis of drought variability and impacts. *Bulletin of the American Meteorological Society*, *91*(10), 1351-1354, doi: 10.1175/2010BAMS2988.1

Beguería, S., Vicente-Serrano, S. M., Reig, F., & Latorre, B. (2014). Standardized precipitation evapotranspiration index (SPEI) revisited: parameter fitting, evapotranspiration models, tools, datasets and drought monitoring. *International journal of climatology*, *34*(10), 3001-3023, doi: 10.1002/joc.3887

Bell, G. D., Halpert, M. S., Ropelewski, C. F., Kousky, V. E., Douglas, A. V., Schnell, R. C., & Gelman, M. E. (1999). Climate assessment for 1998. *Bulletin of the American Meteorological Society*, *80*(5s), S1-S48, doi: 10.1175/1520-0477(1999)080%3C1040:CAF%3E2.0.CO;2

Berg, P., Donnelly, C., and Gustafsson, D. (2018), Near-real-time adjusted reanalysis forcing data for hydrology, Hydrology and Earth System Sciences, 22, 989–1000, doi: 10.5194/hess-22-989-2018.

Berg, A., Lintner, B.R., Findell, K., Seneviratne, S.I., van den Hurk, B., Ducharne, A., Chéruy, F., Hagemann, S., Lawrence, D.M., Malyshev, S., Meier, A. and Gentine, P. (2015). Interannual Coupling between Summertime Surface Temperature and Precipitation over Land: Processes and Implications for Climate Change. *Journal of Climate*, *28*(3), 1308-1328, doi: 10.1175/JCLI-D-14-00324.1

Bergman, D. L., Magnusson, L., Nilsson, J., Vitart, F. (2019). Seasonal forecasting of tropical cyclone landfall using ECMWF's System 4, Weather and Forecasting, 34 (5), 1239-125, doi:10.1175/WAF-D-18-0032.1

Bernard, E., Naveau, P., Vrac, M., & Mestre, O. (2013). Clustering of maxima: Spatial dependencies among heavy rainfall in France. *Journal of climate*, *26*(20), 7929-7937, doi: 10.1175/JCLI-D-12-00836.1

Bevacqua, E., Michele, C. de, Manning, C., Couasnon, A., Ribeiro, A.F.S., Ramos, A.M., Vignotto, E., Bastos, A., Blesić, S., Durante, F., Hillier, J., Oliveira, S.C., Pinto, J.G., Ragno, E., Rivoire, P., Saunders, K., Wiel, K., Wu, W., Zhang, T. and Zscheischler, J. (2021). Guidelines for Studying Diverse Types of Compound Weather and Climate Events. *Earth's Future*, *9*(11), e2021EF002340. doi: 10.1029/2021EF002340

Bieli, M., Camargo, S. J., Sobel, A. H., Evans, J. L., & Hall, T. (2019). A global climatology of extratropical transition. Part I: Characteristics across basins. Journal of Climate, 32(12), 3557-3582, doi: 10.1175/JCLI-D-17-0518.1

Bieli, M., Sobel, A. H., Camargo, S. J., Tippett, M. K. (2020). A statistical model to predict the extratropical transition of tropical cyclones. Weather and Forecasting, 35(2), 451-466, doi: 10.1175/WAF-D-19-0045.1.

Bister, M., & Emanuel, K. A. (1998). Dissipative heating and hurricane intensity. *Meteorology and Atmospheric Physics*, *65*(3), 233-240, doi: 10.1007/BF01030791

Bloomfield, J.P., and Marchant, B.P (2013), Analysis of groundwater drought building on the standardised precipitation index approach, Hydrology and Earth System Sciences, 17(12), 4769-4787, doi: 10.5194/hess-17-4769-2013

Bosart, L. F., & Lackmann, G. M. (1995). Postlandfall tropical cyclone reintensification in a weakly baroclinic environment: A case study of Hurricane David (September 1979). *Monthly Weather Review*, *123*(11), 3268-3291, doi: 10.1175/1520-0493(1995)123<3268:PTCRIA>2.0.CO;2.

Cai, W., McPhaden, M.J., Grimm, A.M., Rodrigues, R.R., Taschetto, A.S., Garreaud, R.D., Dewitte, B., Poveda, G., Ham, Y.-G., Santoso, A., Ng, B., Anderson, W., Wang, G., Geng, T., Jo, H.-S., Marengo, J.A., Alves, L.M., Osman, M., Li, S., Wu, L., Karamperidou, C., Takahashi, K. and Vera, C. (2020). Climate impacts of the El Niño–Southern Oscillation on South America. *Nature Reviews Earth & Environment*, *1*(4), 215-231, doi: 10.1038/s43017-020-0040-3

Ceglar, A., van der Wijngaart, R., Wit, A. de, Lecerf, R., Boogaard, H., Seguini, L., van den Berg, M., Toreti, A., Zampieri, M., Fumagalli, D. and Baruth, B. (2019). Improving WOFOST model to simulate winter wheat phenology in Europe: Evaluation and effects on yield. *Agricultural Systems*, *168*, 168-180, doi: 10.1016/j.agsy.2018.05.002

Chen, M., Shi, W., Xie, P., Silva, V. B., Kousky, V. E., Wayne Higgins, R., & Janowiak, J. E. (2008). Assessing objective techniques for gauge-based analyses of global daily precipitation. *Journal of Geophysical Research: Atmospheres*, *113*(D4), doi: 10.1029/2007JD009132

Chylek, P., Dubey, M. K., Lesins, G., Li, J., & Hengartner, N. (2014). Imprint of the Atlantic multi-decadal oscillation and Pacific decadal oscillation on southwestern US climate: Past, present, and future. *Climate dynamics*, *43*(1), 119-129, doi: 10.1007/s00382-013-1933-3

Coumou, D., Di Capua, G., Vavrus, S., Wang, L., & Wang, S. (2018). The influence of Arctic amplification on mid-latitude summer circulation. *Nature Communications*, 9(1), 1–12. doi:10.1038/s41467-018-05256-8.

Couasnon, A., Sebastian, A., & Morales-Nápoles, O. (2018). A copula-based Bayesian network for modeling compound flood hazard from riverine and coastal interactions at the catchment scale: An application to the Houston Ship Channel, Texas. *Water*, *10*(9), 1190, doi: 10.3390/w10091190

CPCtemp: https://www.esrl.noaa.gov/psd/data/gridded/data.cpc.globaltemp.html, last access: 18 December 2017.

Crespi A., Terzi S., Cocuccioni S., Zebisch M., Berckmans J., Füssel H-M (2020). Climate-related hazard indices for Europe. European Topic Centre on Climate Change impacts, Vulnerability and Adaptation (ETC/CCA) Technical Paper 2020/1.doi: 10.25424/cmcc/climate_related_hazard_indices_europe_2020.

Cronie, O., & Van Lieshout, M. N. M. (2015). AJ-function for inhomogeneous spatio-temporal point processes. *Scandinavian Journal of Statistics*, *42*(2), 562-57, doi: 10.1111/sjos.12123

Cronie, O., & van Lieshout, M. N. M. (2016). Summary statistics for inhomogeneous marked point processes. *Annals of the Institute of Statistical Mathematics*, *68*(4), 905-928, doi: 10.1007/s10463-015-0515-z

Czado, C., & Nagler, T. (2022). Vine copula based modeling. *Annual Review of Statistics and Its Application*, *9*(1), 453-477, doi:

Daley, D.J. (2003), *An Introduction to the Theory of Point Processes: Volume I: Elementary Theory and Methods, Probability and Its Applications Ser,* 2nd ed., Springer New York, New York, NY.

Daley, D.J. and Vere-Jones, D. (2008), *An introduction to the theory of point processes,* Secon edition, Springer, New York.

Datt, I., Camargo, S. J., Sobel, A. H., McTaggart-Cowan, R., Wang, Z. (2022). An Investigation of Tropical Cyclone Development Pathways as an Indicator of Extratropical Transition. Journal of the Meteorological Society of Japan, in press, doi: 10.2151/jmsj.2022-037.

Della-Marta, P. M., Luterbacher, J., von Weissenfluh, H., Xoplaki, E., Brunet, M., & Wanner, H. (2007). Summer heat waves over western Europe 1880–2003, their relationship to large-scale forcings and predictability. *Climate Dynamics*, *29*(2), 251-275. doi:10.1007/s00382-007-0233-1

Diggle, P.J. (2014), *Statistical analysis of spatial and spatio-temporal point patterns, Monographs on statistics and applied probability*, Vol. 128, 3. ed., CRC Press, Boca Raton, Fla.

Domeisen, D. I., and Butler, A. H. (2020), Stratospheric drivers of extreme events at the Earth's surface. *Communications Earth & Environment*, *1*(1), 1-8, doi: 10.1038/s43247-020-00060-z

Dong, L., Mitra, C., Greer, S., & Burt, E. (2018). The dynamical linkage of atmospheric blocking to drought, heatwave and urban heat island in southeastern US: A multi-scale case study. *Atmosphere*, *9*(1), 33, doi: 10.3390/atmos9010033

Donnelly, C., Andersson, J. C., & Arheimer, B. (2016). Using flow signatures and catchment similarities to evaluate the E-HYPE multi-basin model across Europe. *Hydrological Sciences Journal*, *61*(2), 255-273, doi: 10.1080/02626667.2015.1027710

Douville, H., K. Raghavan, J. Renwick, R.P. Allan, P.A. Arias, M. Barlow, R. Cerezo-Mota, A. Cherchi, T.Y. Gan, J. Gergis, D. Jiang, A. Khan, W. Pokam Mba, D. Rosenfeld, J. Tierney, and O. Zolina (2021), Water Cycle Changes. In Climate Change 2021: The Physical Science Basis. Contribution of Working Group I to the Sixth Assessment Report of the Intergovernmental Panel on Climate Change [Masson-Delmotte, V., P. Zhai, A. Pirani, S.L. Connors, C. Péan, S. Berger, N. Caud, Y. Chen, L. Goldfarb, M.I. Gomis, M. Huang, K. Leitzell, E. Lonnoy, J.B.R. Matthews, T.K. Maycock, T. Waterfield, O. Yelekçi, R. Yu, and B. Zhou (eds.)]. Cambridge University Press, Cambridge, United Kingdom and New York, NY, USA, pp. 1055–1210

Duchez, A., Frajka-Williams, E., Josey, S. A., Evans, D. G., Grist, J. P., Marsh, R., ... & Hirschi, J. J. (2016). Drivers of exceptionally cold North Atlantic Ocean temperatures and their link to the 2015 European heat wave. *Environmental Research Letters*, *11*(7), 074004. doi:10.1088/1748-9326/11/7/074004

Dvorak, V. F. (1984). *Tropical cyclone intensity analysis using satellite data* (Vol. 11). US Department of Commerce, National Oceanic and Atmospheric Administration, National Environmental Satellite, Data, and Information Service.

Elidan, G. (2013), “Copulas in Machine Learning”, in Jaworski, P., Durante, F. and Härdle, W.K. (Eds.), *Copulae in mathematical and quantitative finance: Proceedings of the workshop held in Cracow, 10 - 11 July 2012*, *Lecture notes in statistics Proceedings*, Vol. 213, Springer, Berlin, Heidelberg, pp. 39–60.

Emanuel, K., & Nolan, D. S. (2004, July). Tropical cyclone activity and the global climate system. In *26th conference on hurricanes and tropical meteorology*.

Emanuel, K. A. (1988). The maximum intensity of hurricanes. *J. Atmos. Sci*, *45*(7), 1143-1155.

Evans, C., et al. (2017). The Extratropical Transition of Tropical Cyclones. Part I: Cyclone Evolution and Direct Impacts, *Monthly Weather Review*, 145(11), 4317-4344. doi: 10.1175/MWR-D-17-0027.1

Eyring, V., Bony, S., Meehl, G. A., Senior, C. A., Stevens, B., Stouffer, R. J., & Taylor, K. E. (2016). Overview of the Coupled Model Intercomparison Project Phase 6 (CMIP6) experimental design and organization. *Geoscientific Model Development*, *9*(5), 1937-1958, doi: 10.5194/gmd-9-1937-2016

FAO (1983), Guidelines: Land evaluation for rainfed agriculture, FAO Soils Bulletin 52.

Fischer, E. M., & Knutti, R. (2013). Robust projections of combined humidity and temperature extremes. *Nature Climate Change*, *3*(2), 126-130, doi: 10.1038/nclimate1682

Frank, W. M., & Roundy, P. E. (2006). The Role of Tropical Waves in Tropical Cyclogenesis, Monthly Weather Review, 134(9), 2397-2417, doi: 10.1175/MWR3204.1.

Freychet, N., Tett, S., Wang, J., & Hegerl, G. (2017). Summer heat waves over eastern China: Dynamical processes and trend attribution. *Environmental Research Letters*, *12*(2), 024015, doi: 0.1088/1748-9326/aa5ba3

Forootan, E., Khaki, M., Schumacher, M., Wulfmeyer, V., Mehrnegar, N., van Dijk, A. I., et al. (2019),

Understanding the global hydrological droughts of 2003–2016 and their relationships with teleconnections, *Science of the Total Environment*, 650, 2587-2604, doi: 10.1016/j.scitotenv.2018.09.231

García-Martínez, I. M., & Bollasina, M. A. (2021). Identifying the evolving human imprint on heat wave trends over the United States and Mexico. *Environmental Research Letters*, *16*(9), 094039. doi:10.1088/1748-9326/ac1edb

Garrido-Perez J.M., Ordóñez C., Barriopedro D., García-Herrera R., Schnell J.L., Horton D.E. (2022)/ A storyline view of the projected role of remote drivers on summer air stagnation in Europe and the United States. *Environmental Research Letters*, 17(1), 014026. doi: 10.1088/1748-9326/ac4290

Giuliani, M., Crochemore, L., Pechlivanidis, I., & Castelletti, A. (2020). From skill to value: isolating the influence of end user behavior on seasonal forecast assessment. *Hydrology and Earth System Sciences*, *24*(12), 5891-5902, doi: 10.5194/hess-24-5891-2020

Gray, W. M. (1968). Global view of the origin of tropical disturbances and storms. *Monthly Weather Review*, *96*(10), 669-700., doi: 10.1175/1520-0493(1968)096,0669:GVOTOO.2.0.CO;2.

Gray, W. M. (1979). Hurricanes: Their formation, structure and likely role in the tropical circulation. *Meteorology over the tropical oceans*, *155*, 218

Gray, W. M. (1984). Atlantic Seasonal Hurricane Frequency. Part I: El Niño and 30 mb Quasi-Biennial Oscillation Influences. *Monthly Weather Review,* 112(9), 1649-1668, doi:10.1175/1520-0493(1984)112<1649:ASHFPI>2.0.CO;2.

González, J. A., Rodríguez-Cortés, F. J., Cronie, O., & Mateu, J. (2016). Spatio-temporal point process statistics: a review. *Spatial Statistics*, *18*, 505-544, doi: 10.1016/j.spasta.2016.10.002

Hao, Z., Hao, F., Singh, V. P., & Zhang, X. (2019). Statistical prediction of the severity of compound dry-hot events based on El Niño-Southern Oscillation. *Journal of Hydrology*, *572*, 243-250, doi: 10.1016/j.jhydrol.2019.03.001

Hao, Z., Singh, V. P., & Hao, F. (2018). Compound extremes in hydroclimatology: a review. *Water*, *10*(6), 718, doi: 10.3390/w10060718

Hao, Z., & AghaKouchak, A. (2013). Multivariate standardized drought index: a parametric multi-index model. *Advances in Water Resources*, *57*, 12-18, doi: 10.1016/j.advwatres.2013.03.009

Haro, D., Solera, A., Paredes, J., and Andreu, J. (2014), Methodology for drought risk assessment in within-year regulated reservoir systems. Application to the Orbigo river system (Spain), *Water Resources Management*, 28, 3801–3814, doi: 10.1007/s11269-014-0710-3

Hastie, T., Tibshirani, R. and Friedman, J.H. (2017), *The elements of statistical learning: Data mining, inference, and prediction, Springer Series in Statistics,* Second edition, Springer, New York, NY.

Hayes, M. J., Svoboda, M. D., Wiihite, D. A., & Vanyarkho, O. V. (1999). Monitoring the 1996 drought using the standardized precipitation index. *Bulletin of the American meteorological society*, *80*(3), 429-438, doi: 10.1175/1520-0477(1999)080<0429:MTDUTS>2.0.CO;2

Harris, I.C.; Jones, P.D. (2017). CRU TS4.00: Climatic Research Unit (CRU) Time-Series (TS) version 4.00 of high-resolution gridded data of month-by-month variation in climate (Jan. 1901- Dec. 2015). Centre for Environmental Data Analysis, 25 August 2017. doi:10.5285/edf8febfdaad48abb2cbaf7d7e846a86.
doi:10.5285/edf8febfdaad48abb2cbaf7d7e846a86

Hart, R. E. (2003). A cyclone phase space derived from thermal wind and thermal asymmetry. *Monthly weather review*, *131*(4), 585-616. doi:10.1175/1520-0493(2003)131,0585:ACPSDF.2.0.CO;2.

Hart, R. E., & Evans, J. L. (2001). A climatology of the extratropical transition of Atlantic tropical cyclones. *Journal of Climate*, *14*(4), 546-564, doi: 10.1175/1520-0442(2001)014,0546:ACOTET.2.0.CO;2

Hayes, M. J., Svoboda, M. D., Wiihite, D. A., & Vanyarkho, O. V. (1999). Monitoring the 1996 drought using the standardized precipitation index. *Bulletin of the American meteorological society*, *80*(3), 429-438, doi: 10.1175/1520-0477(1999)080<0429:MTDUTS>2.0.CO;2

Henderson, S. A., & Maloney, E. D. (2013). An intraseasonal prediction model of Atlantic and east Pacific tropical cyclone genesis. *Monthly Weather Review*, *141*(6), 1925-1942, doi: 10.1175/MWR-D-12-00268.1.

Hersbach, H., Bell, B., Berrisford, P., Hirahara, S., Horányi, A., Muñoz-Sabater, J., Nicolas, J., Peubey, C., Radu, R., Schepers, D., Simmons, A., Soci, C., Abdalla, S., Abellan, X., Balsamo, G., Bechtold, P., Biavati, G., Bidlot, J., Bonavita, M., … Thépaut, J. (2020). The ERA5 global reanalysis. *Quarterly Journal of the Royal Meteorological Society*, 146(730), 1999–2049.doi: 10.1002/qj.3803

Hill, B. (2012), Understanding the common agricultural policy, *Earthscan*, Milton Park, Abingdon, Oxon, New York, N.Y., 335p., doi: 10.4324/9781849775618

Hoerling, M., Kumar, A., Dole, R., Nielsen-Gammon, J.W., Eischeid, J., Perlwitz, J., Quan, X.-W., Zhang, T., Pegion, P. and Chen, M. (2013), "Anatomy of an Extreme Event", *Journal of Climate*, Vol. 26 No. 9, pp. 2811–2832

Hoerling, M., Kumar, A., Dole, R., Nielsen-Gammon, J. W., Eischeid, J., Perlwitz, J., Quan, X.-W., Zhang, T., Pegion, P. and Chen, M. (2013). Anatomy of an extreme event. *Journal of Climate*, *26*(9), 2811-2832, doi: 10.1175/JCLI-D-12-00270.1

Horton, D. E., Skinner, C. B., Singh, D., & Diffenbaugh, N. S. (2014). Occurrence and persistence of future atmospheric stagnation events. *Nature climate change*, *4*(8), 698-703, doi: 10.1038/nclimate2272

Hundecha, Y., Arheimer, B., Donnelly, C., and Pechlivanidis, I. (2016), A regional parameter estimation scheme for a pan-European multi-basin model, *Journal of Hydrology Regional Studies*, 6, 90–111, doi: 10.1016/j.ejrh.2016.04.002

Ionita, M., Caldarescu, D. E., & Nagavciuc, V. (2021). Compound Hot and Dry Events in Europe: Variability and Large-Scale Drivers. *Frontiers in Climate*, *3*, 688991, doi: 10.3389/fclim.2021.688991

IPCC (2022), "Climate Change 2022: Impacts, Adaptation, and Vulnerability. Contribution of Working Group II to the Sixth Assessment Report of the Intergovernmental Panel on Climate Change [H.-O.

Pörtner, D.C. Roberts, M. Tignor, E.S. Poloczanska, K. Mintenbeck, A. Alegría, M. Craig, S. Langsdorf, S. Löschke, V. Möller, A. Okem, B. Rama (eds.)]", *Cambridge University Press. In Press.*

Janiga, M. A., J. Schreck, C., III, Ridout, J. A., Flatau, M., Barton, N. P., Metzger, E. J., & Reynolds, C. A. (2018). Subseasonal Forecasts of Convectively Coupled Equatorial Waves and the MJO: Activity and Predictive Skill, Monthly Weather Review, 146(8), 2337-2360, doi: 10.1175/MWR-D-17-0261.1.

Jacques-Dumas, V., Ragone, F., Borgnat, P., Abry, P., & Bouchet, F. (2021). Deep Learning-based Extreme Heatwave Forecast. *arXiv preprint arXiv:2103.09743,* doi: 10.48550/arXiv.2103.09743

Jones, S. C., Harr, P. A., Abraham, J., Bosart, L. F., Bowyer, P. J., Evans, J. L., Hanley, D. E., Hanstrum, B. N., Hart, R. E., Lalaurette, F., Sinclair, M. R., Smith, R. K., & Thorncroft, C. (2003). The Extratropical Transition of Tropical Cyclones: Forecast Challenges, Current Understanding, and Future Directions, *Weather and Forecasting*, 18(6), 1052-1092, doi: 10.1175/1520-0434(2003)018<1052:TETOTC>2.0.CO;2.

Jungclaus, J.H., Bard, E., Baroni, M., Braconnot, P., Cao, J., Chini, L.P., Egorova, T., Evans, M., González-Rouco, J.F., Goosse, H., Hurtt, G.C., Joos, F., Kaplan, J.O., Khodri, M., Klein Goldewijk, K., Krivova, N., LeGrande, A.N., Lorenz, S.J., Luterbacher, J., Man, W., Maycock, A.C., Meinshausen, M., Moberg, A., Muscheler, R., Nehrbass-Ahles, C., Otto-Bliesner, B.I., Phipps, S.J., Pongratz, J., Rozanov, E., Schmidt, G.A., Schmidt, H., Schmutz, W., Schurer, A., Shapiro, A.I., Sigl, M., Smerdon, J.E., Solanki, S.K., Timmreck, C., Toohey, M., Usoskin, I.G., Wagner, S., Wu, C.-J., Yeo, K.L., Zanchettin, D., Zhang, Q. and Zorita, E. (2017). The PMIP4 contribution to CMIP6–Part 3: The last millennium, scientific objective, and experimental design for the PMIP4 past1000 simulations. *Geoscientific Model Development*, *10*(11), 4005-4033, doi: 10.5194/gmd-10-4005-2017

Katsafados, P., Papadopoulos, A., Varlas, G., Papadopoulou, E., & Mavromatidis, E. (2014). Seasonal predictability of the 2010 Russian heat wave. *Natural Hazards and Earth System Sciences*, *14*(6), 1531-1542., doi: 10.5194/nhess-14-1531-2014

Keller, J. H., et al. (2019). The Extratropical Transition of Tropical Cyclones. Part II: Interaction with the Midlatitude Flow, Downstream Impacts, and Implications for Predictability, *Monthly Weather Review*, 147(4), 1077-1106, doi:10.1175/MWR-D-17-0329.1

Kendrovski, V., Baccini, M., Martinez, G. S., Wolf, T., Paunovic, E., & Menne, B. (2017). Quantifying projected heat mortality impacts under 21st-century warming conditions for selected European countries. *International journal of environmental research and public health*, *14*(7), 729, doi:10.3390/ijerph14070729.

Kenyon, J., & Hegerl, G. C. (2008). Influence of modes of climate variability on global temperature extremes. *Journal of Climate*, *21*(15), 3872-3889, doi:10.1175/2008JCLI2125.1

Kiladis, G. N., Wheeler, M. C., Haertel, P. T., Straub, K. H., and Roundy, P. E. (2009), Convectively coupled equatorial waves, *Rev. Geophys.*, 47, RG2003, doi: 10.1029/2008RG000266.

Klein, P. M., Harr, P. A., & Elsberry, R. L. (2000). Extratropical Transition of Western North Pacific Tropical Cyclones: An Overview and Conceptual Model of the Transformation Stage, *Weather and Forecasting*, 15(4), 373-395, doi: 10.1175/1520-0434(2000)015<0373:ETOWNP>2.0.CO;2.

Klotzbach, P. J. (2014). The Madden–Julian oscillation's impacts on worldwide tropical cyclone activity. *Journal of Climate*, 27(6), 2317–2330, doi:/10.1175/JCLI-D-13-00483.1

Knapp, K. R., Kruk, M. C., Levinson, D. H., Diamond, H. J., & Neumann, C. J. (2010). The international best track archive for climate stewardship (Ibtracs): Unifying tropical cyclone data. *Bulletin of the American Meteorological Society*, 91(3), 363–376, doi:10.1175/2009BAMS2755.1

Kornhuber, K., Osprey, S., Coumou, D., Petri, S., Petoukhov, V., Rahmstorf, S., & Gray, L. (2019). Extreme weather events in early summer 2018 connected by a recurrent hemispheric wave-7 pattern. *Environmental Research Letters*, *14*(5), 054002. doi:10.1088/1748-9326/ab13bf

Kornhuber, K., Coumou, D., Vogel, E., Lesk, C., Donges, J. F., Lehmann, J., & Horton, R. M. (2020). Amplified Rossby waves enhance risk of concurrent heatwaves in major breadbasket regions. *Nature Climate Change*, *10*(1), 48-53, doi:10.1038/s41558-019-0637-z

Lau, N. C., & Nath, M. J. (2012). A model study of heat waves over North America: Meteorological aspects and projections for the twenty-first century. *Journal of Climate*, *25*(14), 4761-4784. doi:10.1175/JCLI-D-11-00575.1

Lawton, Q. A., Majumdar, S. J., Dotterer, K., Thorncroft, C., & Schreck III, C. J. (2022). The influence of convectively coupled kelvin waves on african easterly waves in a wave-following framework. *Monthly Weather Review*. doi:10.1175/MWR-D-21-0321.1

Leonard, M., Westra, S., Phatak, A., Lambert, M., van den Hurk, B., McInnes, K., Risbey, J., Schuster, S., Jakob, D. and Stafford-Smith, M. (2014). A compound event framework for understanding extreme impacts. *Wiley Interdisciplinary Reviews: Climate Change*, *5*(1), 113-128, doi: 10.1002/wcc.252

Leroy, A., & Wheeler, M. C. (2008). Statistical Prediction of Weekly Tropical Cyclone Activity in the Southern Hemisphere, *Monthly Weather Review*, 136(10), 3637-3654, doi:10.1175/2008MWR2426.1.

Lesk, C., Rowhani, P., & Ramankutty, N. (2016). Influence of extreme weather disasters on global crop production. Nature, 529(7584), 84–87. doi:10.1038/nature16467

Lindström, C., Åman, J., & Norberg, A. L. (2010). Increased prevalence of burnout symptoms in parents of chronically ill children. *Acta paediatrica*, *99*(3), 427-432. doi: 10.1111/j.1651-2227.2009.01586.x.

Loikith, P. C., & Broccoli, A. J. (2012). Characteristics of observed atmospheric circulation patterns associated with temperature extremes over North America. *Journal of Climate*, *25*(20), 7266-7281. doi:10.1175/JCLI-D-11-00709.1

Lorenz, R., Davin, E. L., Lawrence, D. M., Stöckli, R., & Seneviratne, S. I. (2013). How important is vegetation phenology for European climate and heat waves?. *Journal of Climate*, *26*(24), 10077-10100. doi:10.1175/JCLI-D-13-00040.1

Luo, M., Lau, N. C., & Liu, Z. (2022). Different mechanisms for daytime, nighttime, and compound heatwaves in Southern China. *Weather and Climate Extremes*, 100449. doi:10.1016/j.wace.2022.100449

Magnusson, L. et al. (2021). Tropical cyclone activities at ECMWF. ECMWF Technical Memorandum 888.

Maier-Gerber, M., Fink, A. H., Riemer, M., Schoemer, E., Fischer, C., & Schulz, B. (2021). Statistical-Dynamical Forecasting of Subseasonal North Atlantic Tropical Cyclone Occurrence. *Weather and Forecasting*, *36*(6), 2127-2142, doi:10.1175/WAF-D-21-0020.1

Materia, S., Ardilouze, C., Prodhomme, C., Donat, M. G., Benassi, M., Doblas-Reyes, F. J., ... & Gualdi, S. (2021). Summer temperature response to extreme soil water conditions in the Mediterranean transitional climate regime. *Climate Dynamics*, 1-21. doi:10.1007/s00382-021-05815-8

Matsueda, M. (2011). Predictability of Euro-Russian blocking in summer of 2010. *Geophysical Research Letters*, *38*(6). doi:10.1029/2010GL046557

Matsuno, T. (1966), Quasi-geostrophic motions in the equatorial area, *Journal of the Meteorological Society of Japan*., 44, 25–43, doi:10.2151/jmsj1965.44.1_25.

McKee, T. B., Doesken, N. J., & Kleist, J. (1993, January). The relationship of drought frequency and duration to time scales. In *Proceedings of the 8th Conference on Applied Climatology*(Vol. 17, No. 22, pp. 179-183).

McTaggart-Cowan, R., Davies, E. L., Fairman Jr, J. G., Galarneau Jr, T. J., & Schultz, D. M. (2015). Revisiting the 26.5° C sea surface temperature threshold for tropical cyclone development. *Bulletin of the American Meteorological Society*, 96 (11), 1929-1943, doi:10.1175/BAMS-D-13-00254.1.

McTaggart-Cowan, R., Deane, G. D., Bosart, L. F., Davis, C. A., & Galarneau, T. J., Jr. (2008). Climatology of Tropical Cyclogenesis in the North Atlantic (1948–2004), *Monthly Weather Review*, 136(4), 1284-1304, doi: 10.1175/2007MWR2245.1.

McTaggart-Cowan, R., Galarneau, T. J., Jr., Bosart, L. F., Moore, R. W., & Martius, O. (2013). A Global Climatology of Baroclinically Influenced Tropical Cyclogenesis, Monthly Weather Review, 141(6), 1963-1989, doi:10.1175/MWR-D-12-00186.1.

McTaggart-Cowan, R., Gyakum, J. R., & Yau, M. K. (2003). The Influence of the Downstream State on Extratropical Transition: Hurricane Earl (1998) Case Study, *Monthly Weather Review,* 131(8), 1910-1929, doi:10.1175//2589.1.

Meng, Y., Hao, Z., Feng, S., Zhang, X., & Hao, F. (2022). Increase in compound dry-warm and wet-warm events under global warming in CMIP6 models. *Global and Planetary Change*, *210*, 103773, doi: 10.1016/j.gloplacha.2022.103773

MIDAS @ JRC website 2021 (2021), "PRIMES Energy System Model", available at: https://web.jrc.ec.europa.eu/policy-model-inventory/explore/models/model-primes (accessed 4 July 2022).

Miralles, D. G., Gentine, P., Seneviratne, S. I., & Teuling, A. J. (2019). Land–atmospheric feedbacks during droughts and heat waves: state of the science and current challenges. Annals of the New York Academy of Sciences, 1436(1), 19–35. doi:10.1111/nyas.13912

Mishra, A.K. and Singh, V.P. (2010), A review of drought concepts, *Journal of Hydrology*, 391, 202-216, doi:10.1016/j.jhydrol.2010.07.012

Moradi, M. M., Cronie, O., Rubak, E., Lachieze-Rey, R., Mateu, J., & Baddeley, A. (2019). Resample-smoothing of Voronoi intensity estimators. *Statistics and computing*, *29*(5), 995-1010, doi: 10.1007/s11222-018-09850-0

Mukherjee, S., Ashfaq, M., & Mishra, A. K. (2020). Compound drought and heatwaves at a global scale: The role of natural climate variability-associated synoptic patterns and land-surface energy budget anomalies. *Journal of Geophysical Research: Atmospheres*, *125*(11), e2019JD031943.

Palmen, E., 1948: On the formation and structure of tropical hurricanes. *Geophysica*, 3, 26–38.

Palmer, W. C. (1965). *Meteorological drought* (Vol. 30). US Department of Commerce, Weather Bureau.

Papin, P. P., Bosart, L. F., & Torn, R. D. (2020). A Feature-Based Approach to Classifying Summertime Potential Vorticity Streamers Linked to Rossby Wave Breaking in the North Atlantic Basin, *Journal of Climate*, 33(14), 5953-5969, doi:10.1175/JCLI-D-19-0812.1.

Pedro-Monzonís, M., Solera, A., Ferrer, J., Estrela, T., & Paredes-Arquiola, J. (2015). A review of water scarcity and drought indexes in water resources planning and management. *Journal of Hydrology*, *527*, 482-493, doi: 10.1016/j.jhydrol.2015.05.003

Perkins-Kirkpatrick, S. E., & Lewis, S. C. (2020). Increasing trends in regional heatwaves. *Nature Communications*, 11(1). doi:10.1038/s41467-020-16970-7

Poli, P., Hersbach, H., Dee, D.P., Berrisford, P., Simmons, A.J., Vitart, F., Laloyaux, P., Tan, D.G.H., Peubey, C., Thépaut, J.-N., Trémolet, Y., Hólm, E.V., Bonavita, M., Isaksen, L. and Fisher, M. ((2016).

ERA-20C: An atmospheric reanalysis of the twentieth century. *Journal of Climate*, *29*(11), 4083-4097, doi: 10.1175/JCLI-D-15-0556.1

PRIMES (2018), PRIMES Model version 2018. Detailed model description, available at: https://e3modelling.com/modelling-tools/primes/ (accessed 5 July 2022).

Prodhomme, C., Materia, S., Ardilouze, C., White, R. H., Batté, L., Guemas, V., Fragkoulidis, G., & García-Serrano, J. (2022). Seasonal prediction of European summer heatwaves. *Climate Dynamics*, *58*(7), 2149-2166. doi:10.1007/s00382-021-05828-3

Quesada, B., Vautard, R., Yiou, P., Hirschi, M., & Seneviratne, S. I. (2012). Asymmetric European summer heat predictability from wet and dry southern winters and springs. *Nature Climate Change*, *2*(10), 736-741.doi:10.1038/nclimate1536

Raymond, C., Horton, R.M., Zscheischler, J., Martius, O., AghaKouchak, A., Balch, J., Bowen, S.G., Camargo, S.J., Hess, J., Kornhuber, K., Oppenheimer, M., Ruane, A.C., Wahl, T. and White, K. (2020 Understanding and managing connected extreme events. *Nature climate change*, *10*(7), 611-621, doi: 0.1038/s41558-020-0790-4

Reddy, P. J., Perkins-Kirkpatrick, S. E., Ridder, N. N., & Sharples, J. J. (2022). Combined role of ENSO and IOD on compound drought and heatwaves in Australia using two CMIP6 large ensembles. *Weather and Climate Extremes*, 100469, doi: 10.1016/j.wace.2022.100469

Ritchie, E. A., & Elsberry, R. L. (2003). Simulations of the Extratropical Transition of Tropical Cyclones: Contributions by the Midlatitude Upper-Level Trough to Reintensification, Monthly Weather Review, 131(9), 2112-2128, doi:10.1175/1520-0493(2003)131<2112:SOTETO>2.0.CO;2.

Ritchie, E. A., & Elsberry, R. L. (2007). Simulations of the extratropical transition of tropical cyclones: Phasing between the upper-level trough and tropical cyclones. *Monthly weather review*, *135*(3), 862-876, doi:10.1175/MWR3303.1.

Roberts, M. J., J. Camp, J. Seddon, P. L. Vidale, K. Hodges, B. Vanniere, J. Mecking, R. Haarsma, A. Bellucci, E. Scoccimarro, L.-P. Caron, F. Chauvin, L. Terray, S. Valcke, M.-P. Moine, D. Putrasahan, C. Roberts, R. Senan, C. Zarzycki, P. Ullrich, (2020). Impact of model resolution on tropical cyclone simulation using the HighResMIP–PRIMAVERA multimodel ensemble. *Journal of Climate*, *33*(7), 2557-2583. doi:10.1175/JCLI-D-19-0639.1

Russo, S., Dosio, A., Graversen, R. G., Sillmann, J., Carrao, H., Dunbar, M. B., ... & Vogt, J. V. (2014). Magnitude of extreme heat waves in present climate and their projection in a warming world. *Journal of Geophysical Research: Atmospheres*, *119*(22), 12-500. doi:10.1002/2014JD022098

Russo, S., Sillmann, J., and Fischer, E.M. (2015). Top ten European heatwaves since 1950 and their occurrence in the coming decades. *Environmental Research Letters, 10*(12), 124003. doi:10.1088/1748-9326/10/12/124003

Russo, S., Sillmann, J., & Sterl, A. (2017). Humid heat waves at different warming levels. *Scientific reports*, *7*(1), 1-7. doi:10.1038/s41598-017-07536-7

Sainsbury, E. M., Schiemann, R. K. H., Hodges, K. I., Shaffrey, L. C., Baker, A. J., & Bhatia, K. T. (2020). How Important Are Post-Tropical Cyclones for European Windstorm Risk? *Geophysical Research Letters*, 47(18). doi:10.1029/2020GL089853

Sainsbury, E. M., Schiemann, R. K. H., Hodges, K. I., Baker, A. J., Shaffrey, L. C., & Bhatia, K. T. (2022). Why do some post-tropical cyclones impact Europe? *Monthly Weather Review*, 150(10), 2553–2571. doi:10.1175/MWR-D-22-0111.1

Schäfler, A., Craig, G., Wernli, H., Arbogast, P., Doyle, J.D., McTaggart-Cowan, R., Methven, J., Rivière, G., Ament, F., Boettcher, M. and Bramberger, M. (2018). The North Atlantic waveguide and downstream impact experiment. *Bulletin of the American Meteorological Society*, *99*(8), 1607-1637, doi:10.1175/BAMS-D-17-0003.1

Schaller, N., Sillmann, J., Anstey, J., Fischer, E. M., Grams, C. M., & Russo, S. (2018). Influence of blocking on Northern European and Western Russian heatwaves in large climate model ensembles. *Environmental Research Letters*, *13*(5), 054015. doi:10.1088/1748-9326/aaba55

Schreck, C. J., III, Molinari, J., & Aiyyer, A. (2012). A Global View of Equatorial Waves and Tropical Cyclogenesis, *Monthly Weather Review*, 140(3), 774-788, doi:10.1175/MWR-D-11-00110.1.

Schreck, C. J., III, Molinari, J., & Mohr, K. I. (2011). Attributing Tropical Cyclogenesis to Equatorial Waves in the Western North Pacific, *Journal of the Atmospheric Sciences*, 68(2), 195-209, doi:10.1175/2010JAS3396.1.

Schneider, U., Becker, A., Finger, P., Meyer-Christoffer, A., Ziese, M., & Rudolf, B. (2014). GPCC's new land surface precipitation climatology based on quality-controlled in situ data and its role in quantifying the global water cycle. *Theoretical and Applied Climatology*, *115*(1), 15-40, doi: 10.1007/s00704-013-0860-x

Schumacher, D. L., Keune, J., Van Heerwaarden, C. C., Vilà-Guerau de Arellano, J., Teuling, A. J., & Miralles, D. G. (2019). Amplification of mega-heatwaves through heat torrents fuelled by upwind drought. *Nature Geoscience*, *12*(9), 712-717, doi: 10.1038/s41561-019-0431-6

Scoccimarro, E., Fogli, P. G., & Gualdi, S. (2017). The role of humidity in determining scenarios of perceived temperature extremes in Europe. *Environmental Research Letters*, *12*(11), 114029. doi:10.1088/1748-9326/aa8cdd

Seneviratne, S. I., Lüthi, D., Litschi, M., & Schär, C. (2006). Land–atmosphere coupling and climate change in Europe. *Nature*, *443*(7108), 205-209, doi: 10.1038/nature05095

Shukla, S., & Wood, A. W. (2008). Use of a standardized runoff index for characterizing hydrologic drought. *Geophysical research letters*, *35*(2), doi: 10.1029/2007GL032487

Sillmann, J., Thorarinsdottir, T., Keenlyside, N., Schaller, N., Alexander, L. V., Hegerl, G., ... & Zwiers, F. W. (2017). Understanding, modeling and predicting weather and climate extremes: Challenges and opportunities. *Weather and climate extremes*, *18*, 65-74. doi:10.1016/j.wace.2017.10.003

Slivinski, L.C., Compo, G.P., Whitaker, J.S., Sardeshmukh, P.D., Giese, B.S., McColl, C., Allan, R., Yin, X., Vose, R., Titchner, H., Kennedy, J., Spencer, L.J., Ashcroft, L., Brönnimann, S., Brunet, M., Camuffo, D., Cornes, R., Cram, T.A., Crouthamel, R., Domínguez-Castro, F., Freeman, J.E., Gergis, J., Hawkins, E., Jones, P.D., Jourdain, S., Kaplan, A., Kubota, H., Le Blancq, F., Lee, T.-C., Lorrey, A., Luterbacher, J., Maugeri, M., Mock, C.J., Moore, G.K., Przybylak, R., Pudmenzky, C., Reason, C., Slonosky, V.C., Smith, C.A., Tinz, B., Trewin, B., Valente, M.A., Wang, X.L., Wilkinson, C., Wood, K. and Wyszyński, P. (2019). Towards a more reliable historical reanalysis: Improvements for version 3 of the Twentieth Century Reanalysis system. *Quarterly Journal of the Royal Meteorological Society*, *145*(724), 2876-2908, doi: 10.1002/qj.3598

Song, J., Klotzbach, P. J., & Duan, Y. (2022). Statistical linkage between coastal El Niño–Southern Oscillation and tropical cyclone formation over the western North Pacific. *Atmospheric Science Letters*, 23(2). doi:10.1002/asl.1071

Sousa P.M., Trigo R. M., Barriopedro D., Soares P. M. M., Santos J. A. (2018). European temperature responses to blocking and ridge regional patterns. *Climate Dynamics*, 50, 1-2, 457-477, doi: 10.1007/s00382-017-3620-2

Sperotto, A., Molina, J.-L., Torresan, S., Critto, A. and Marcomini, A. (2017). Reviewing Bayesian Networks potentials for climate change impacts assessment and management: A multi-risk perspective, *Journal of environmental management*, *202*, 320-331, doi: /10.1016/j.jenvman.2017.07.044

Spinoni, J., Naumann, G., Vogt, J.V., and Barbosa P. (2016), Meteorological droughts in Europe: Events and impacts-past trends and future projections. Publications Office of the European Union, ISBN-13: 978-92-79-55097-3

Spinoni, J., Vogt, J.V., Naumann, G., Barbosa, P., and Dosio, A. (2018). Will drought events become more frequent and severe in Europe? *International Journal of Climatology*, 38(4), 1718-1736, doi: 10.1002/joc.5291

Staudinger, M., Stahl, K., and Seibert, J. (2014), A drought index accounting for snow, *Journal of Hydrology,* 6, 2108–2123, doi:10.1002/2012WR013085

Steinemann, A. C., Hayes, M. J., & Cavalcanti, L. F. (2005). Drought indicators and triggers. *Drought and Water Crises: Science, Technology, and Management Issues, Wilhite DA (ed)*, 71-92

Svoboda, M.D., and Fuchs, B.A. (2016), Handbook of drought indicators and indices, World Meteorological Organization, Geneva

Thomas, N. P., Bosilovich, M. G., Marquardt Collow, A. B., Koster, R. D., Schubert, S. D., Dezfuli, A., & Mahanama, S. P. (2020). Mechanisms associated with daytime and nighttime heat waves over the contiguous United States. *Journal of Applied Meteorology and Climatology*, *59*(11), 1865-1882. doi:10.1175/JAMC-D-20-0053.1

Thorncroft, C. D., Hoskins, B. J., & McIntyre, M. E. (1993). Two paradigms of baroclinic-wave life-cycle behaviour. *Quarterly Journal of the Royal Meteorological Society*, *119*(509), 17-55, doi:10.1002/qj.49711950903.

Tippett, M. K., Camargo, S. J., & Sobel, A. H. (2011). A Poisson regression index for tropical cyclone genesis and the role of large-scale vorticity in genesis. *Journal of Climate*, *24*(9), 2335-2357, doi: 10.1175/2010JCLI3811.1

Toreti, A., Belward, A., Perez-Dominguez, I., Naumann, G., Luterbacher, J., Cronie, O., Seguini, L., Manfron, G., Lopez-Lozano, R., Baruth, B., Berg, M., Dentener, F., Ceglar, A., Chatzopoulos, T. and Zampieri, M. (2019a), The exceptional 2018 European water seesaw calls for action on adaptation. *Earth's Future*, *7*(6), 652-663, doi: 10.1029/2019EF001170

Toreti, A., Cronie, O., & Zampieri, M. (2019b). Concurrent climate extremes in the key wheat producing regions of the world. *Scientific reports*, *9*(1), 1-8, doi: 10.1038/s41598-019-41932-5

Toreti, A., Maiorano, A., Sanctis, G. de, Webber, H., Ruane, A.C., Fumagalli, D., Ceglar, A., Niemeyer, S. and Zampieri, M. (2019c), Using reanalysis in crop monitoring and forecasting systems. *Agricultural systems*, *168*, 144-153, doi: 10.1016/j.agsy.2018.07.001

Troup, A. J. (1965). The 'southern oscillation'. *Quarterly Journal of the Royal Meteorological Society*, *91*(390), 490-506,doi:10.1002/qj.49709139009.

Tsanis, I., and Tapoglou, E (2019), Winter North Atlantic Oscillation impact on European precipitation and drought under climate change, *Theoretical and Applied Climatology*, 135(1), 323-330, doi: 10.1007/s00704-018-2379-7

Van Lieshout, M. N. M. (2011). AJ–function for inhomogeneous point processes. *Statistica Neerlandica*, *65*(2), 183-201, doi: 10.1111/j.1467-9574.2011.00482.x

Vicente-Serrano, S.M., Beguería, S., and López-Moreno, J.I. (2010), A multiscalar drought index sensitive to global warming: the standardized precipitation evapotranspiration index, *Journal of Climate* 23 (7), 1696–1718, doi: 10.1175/2009JCLI2909.1

Vicente-Serrano, S.M., López-Moreno, J.I., Beguería, S., Lorenzo-Lacruz, J., Azorin-Molina, C., Morán-Tejeda, E. (2011), Accurate computation of a streamflow drought index, *Journal of Hydrologic Engineering,* 17 (2), 318–332, doi: 10.1061/(ASCE)HE.1943-5584.0000433

Vicente-Serrano, S. M., López-Moreno, J. I., Gimeno, L., Nieto, R., Morán-Tejeda, E., Lorenzo-Lacruz, J., et al. (2011), A multiscalar global evaluation of the impact of ENSO on droughts, *Journal of Geophysical Research: Atmospheres*, 116(D20), doi: 10.1029/2011JD016039

Vicente-Serrano, S. M., McVicar, T. R., Miralles, D. G., Yang, Y., & Tomas-Burguera, M. (2020), Unraveling the influence of atmospheric evaporative demand on drought and its response to climate change, Wiley Interdisciplinary Reviews: Climate Change, 11(2), doi: 10.1002/wcc.632

Vitart, F., 2009: Impact of the Madden Julian Oscillation on tropical storms and risk of landfall in the ECMWF forecast system. *Geophysical Research Letters*, 36, L15802, doi:10.1029/2009GL039089

Vogel, M. M., Zscheischler, J., Wartenburger, R., Dee, D., & Seneviratne, S. I. (2019). Concurrent 2018 hot extremes across Northern Hemisphere due to human‐induced climate change. *Earth's future*, *7*(7), 692-703, doi: 10.1029/2019EF001189

Vogel, M. M., Hauser, M., & Seneviratne, S. I. (2020). Projected changes in hot, dry and wet extreme events' clusters in CMIP6 multi-model ensemble. *Environmental Research Letters*, *15*(9), 094021, doi: 10.1088/1748-9326/ab90a7

Wahl, T., Jain, S., Bender, J., Meyers, S. D., & Luther, M. E. (2015). Increasing risk of compound flooding from storm surge and rainfall for major US cities. *Nature Climate Change*, *5*(12), 1093-1097, doi: 10.1038/nclimate2736

Wallman, P., Arheimer, B., Isberg, K., Donnelly, C. and Dahné, J. (2011), "E-HYPE and E-HypeWeb Services for Water and Climate Information", available at: https://www.earthobservations.org/documents/meetings/201111_geo8_eu/GEOLAND,%20SUDPLAN%20et%20al.%20Patrick%20Wallman.pdf (accessed 13 July 2022).

Wang, Z., Zhang, G., Dunkerton, T. J., & Jin, F. F. (2020). Summertime stationary waves integrate tropical and extratropical impacts on tropical cyclone activity. *Proceedings of the National Academy of Sciences*, *117*(37), 22720-22726, doi:10.1073/pnas.2010547117.

Wang, P., Yang, Y., Tang, J., Leung, L. R., & Liao, H. (2021). Intensified humid heat events under global warming. *Geophysical Research Letters*, *48*(2), e2020GL091462, doi: 10.1029/2020GL091462

Wheeler, M. C., & Hendon, H. H. (2004). An all-season real-time multivariate MJO index: Development of an index for monitoring and prediction. *Monthly weather review*, *132*(8), 1917-1932, doi:10.1175/1520-0493(2004)132<1917:AARMMI>2.0.CO;2

Wit, A. de, Boogaard, H., Fumagalli, D., Janssen, S., Knapen, R., van Kraalingen, D., Supit, I., van der Wijngaart, R. and van Diepen, K. (2019), 25 years of the WOFOST cropping systems model. *Agricultural systems*, *168*, 154-167, doi: 10.1016/j.agsy.2018.06.018

White, R. H., Kornhuber, K., Martius, O., & Wirth, V. (2022). From Atmospheric Waves to Heatwaves: A Waveguide Perspective for Understanding and Predicting Concurrent, Persistent, and Extreme

Extratropical Weather. *Bulletin of the American Meteorological Society*, *103*(3), E923-E935. doi:10.1175/BAMS-D-21-0170.1

WMO (1986), Report on Drought and Countries Affected by Drought During 1974-1985, World Meteorological Organization, Geneva.

Wulff, C. O., Greatbatch, R. J., Domeisen, D. I., Gollan, G., & Hansen, F. (2017). Tropical forcing of the summer East Atlantic pattern. *Geophysical Research Letters*, *44*(21), 11-166, doi:10.1002/2017GL075493

Yang, W., Andréasson, J., Phil Graham, L., Olsson, J., Rosberg, J., and Wetterhall, F. (2010), Distribution-based scaling to improve usability of regional climate model projections for hydrological climate change impacts studies, *Hydrology Research*, 41, 211–229, doi: 10.2166/nh.2010.004

ZAMCON (2015). *Status Report on Integrated Flood and Drought Mapping in the Zambezi River Basin*. ZAMCOM, SADC Water Division. SARDC IMERCSA. Gaborone, Harare

Zampieri, M., Ceglar, A., Dentener, F., and Toreti, A. (2017). Wheat yield loss attributable to heat waves, drought and water excess at the global, national and subnational scales. *Environmental Research Letters, 12* (6), 064008. doi:10.1088/1748-9326/aa723b

Zargar, A., Sadiq, R., Naser, B., & Khan, F. I. (2011). A review of drought indices. *Environmental Reviews*, *19*(NA), 333-349, doi: 10.1139/a11-013

Zhang, G., Wang, Z., Dunkerton, T. J., Peng, M. S., & Magnusdttir, G. (2016). Extratropical Impacts on Atlantic Tropical Cyclone Activity, *Journal of the Atmospheric Sciences*, 73(3), 1401-1418, doi:10.1175/JAS-D-15-0154.1.

Zhang, G., Wang, Z., Peng, M. S., & Magnusdottir, G. (2017). Characteristics and Impacts of Extratropical Rossby Wave Breaking during the Atlantic Hurricane Season, *Journal of Climate*, 30(7), 2363-2379, doi:10.1175/JCLI-D-16-0425.1.

Zhang, W., Luo, M., Gao, S., Chen, W., Hari, V., & Khouakhi, A. (2021). Compound hydrometeorological extremes: drivers, mechanisms and methods. *Frontiers in Earth Science*, *9*, 673495, doi: 10.3389/feart.2021.67349

Zhu, J., Huang, B., Cash, B., Kinter, J. L., Manganello, J., Barimalala, R., ... & Towers, P. (2015). ENSO prediction in Project Minerva: Sensitivity to atmospheric horizontal resolution and ensemble size. *Journal of Climate*, *28*(5), 2080-2095. doi:10.1175/JCLI-D-14-00302.1.

Zou, Y., Wang, Y., Xie, Z., Wang, H., & Rasch, P. J. (2020). Atmospheric teleconnection processes linking winter air stagnation and haze extremes in China with regional Arctic sea ice decline. *Atmospheric Chemistry and Physics*, *20*(8), 4999-5017, doi: 10.5194/acp-20-4999-2020

Zscheischler, J., & Fischer, E. M. (2020). The record-breaking compound hot and dry 2018 growing season in Germany. *Weather and Climate Extremes*, *29*, 100270, doi: 10.1016/j.wace.2020.100270

Zscheischler, J., Martius, O., Westra, S., Bevacqua, E., Raymond, C., Horton, R.M., van den Hurk, B., AghaKouchak, A., Jézéquel, A., Mahecha, M.D., Maraun, D., Ramos, A.M., Ridder, N.N., Thiery, W. and Vignotto, E. (2020), A typology of compound weather and climate events. *Nature reviews earth & environment*, *1*(7), 333-347, doi: 10.1038/s43017-020-0060-z

Zscheischler, J., & Seneviratne, S. I. (2017). Dependence of drivers affects risks associated with compound events. *Science advances*, *3*(6), e1700263, doi: 10.1126/sciadv.1700263

Zscheischler, J., Westra, S., van den Hurk, B.J.J.M., Seneviratne, S.I., Ward, P.J., Pitman, A., AghaKouchak, A., Bresch, D.N., Leonard, M., Wahl, T. and Zhang, X. (2018). Future climate risk from compound events. *Nature Climate Change*, *8*(6), 469-477, doi: 10.1038/s41558-018-0156-3

Zuo, J., Pullen, S., Palmer, J., Bennetts, H., Chileshe, N., & Ma, T. (2015). Impacts of heat waves and corresponding measures: a review. *Journal of Cleaner Production*, *92*, 1-12. doi: 10.1016/j.jclepro.201

CLINT
CLIMATE INTELLIGENCE

This project is part of the H2020 Programme supported by the European Union, having received funding from it under Grant Agreement No 101003876